Reactive and Functional Polymers 193 (2023) 105763

Contents lists available at ScienceDirect

Reactive and Functional Polymers

journal homepage: www.elsevier.com/locate/react

Green surface modification of polyvinyl alcohol fibers and its application for dye removal using Doehlert experimental design

Eya Ben Khalifa [a], Claudio Cecone [a,*], Boutheina Rzig [b], Soulaima Azaiez [c], Federico Cesano [a], Mery Malandrino [a], Pierangiola Bracco [a], Giuliana Magnacca [a]

[a] Department of Chemistry and NIS Interdepartmental Centre, Torino University, Via P. Giuria 7, 10125 Torino, Italy
[b] Ecochimie Laboratory, National Institute of Applied Sciences and Technology (INSAT), University of Carthage, Tunis, Tunisia
[c] Research Laboratory Desalination and Water Treatment LR19ES01, Faculty of Sciences of Tunis, University of Tunis El Manar 2092, Tunis, Tunisia

ARTICLE INFO

Keywords:
L-cysteine
Polyvinyl alcohol
Fibers
Adsorption
Crystal violet

ABSTRACT

The use of eco-friendly techniques and green reagents to modify the properties of synthetic biopolymers is attracting an increasing attention. In this work, L-cysteine (CYS) modified polyvinyl alcohol electrospun fibers (PVA-CYS) were prepared using an easy, fast, and green technique. The incorporation of CYS as a source of nitrogen and sulfur shows an important enhancement in dye removal efficiency compared to polyvinyl alcohol fibers (PVA). The successful grafting of CYS on PVA was proved by FTIR, elemental analysis, SEM, AFM and TGA analysis. Doehlert experimental design was used to optimize the adsorption process of crystal violet (CV) on PVA and PVA-CYS. The two models show good correlations between experimental and predicted responses, with coefficients of determination equal to 0.946 and 0.976, for PVA and PVA-CYS, respectively. The most influencing parameter was the pH for CV removal by adsorption on PVA. However, this parameter affects less the dye removal using PVA-CYS. The modified fibers exhibit excellent adsorption ability toward CV, and the maximum adsorption capacity reaches 197 mg g^{-1} at neutral pH. An application of this process on a doped real wastewater demonstrates its efficacity and selectivity with a percentage of removal up to 85%.

1. Introduction

Global dyes and pigments market was valued at 36.4 billion dollars in 2021 and is expected to expand at a compound annual growth rate (CAGR) of 5.2% from 2022 to 2030. Increasing demand from various industries, such as paints, coatings, construction, plastics, and textiles is expected to drive market growth [1]. These industries consume a high amount of water and produce a huge quantities of polluted and toxic wastewater [2,3]. >100,000 types of textile dyes are present in the market and approximately 700,000 to 1,000,000 tons of dyes are produced while 280,000 tons of them are discharged annually [4]. Most of the cationic dyes are difficult to degrade in water because of their aromatic structure and they have mutagenic and carcinogenic properties, which are considered as emergent dangers to the environment, marine life, and human health [5,6]. Crystal violet (CV) is a synthetic cationic dye also known as aniline violet, gentian violet, or pyocyanin (Fig. 1). It is widely used in medicine applications as a biological stain, colorant, bacteriostatic and antimicrobial agent [7]. It is also employed as a purple dye in textile industries such as cotton and silk, and to provide a deep violet color in painting and printing [8]. CV has been reported as a recalcitrant dye that persists in the environment for long periods and poses toxic effects on the ecosystem [9]. It affects the aquatic environment by reducing light penetration through water surface [10]. This dye is absorbed easily through the skin and causes both skin and digestive tract irritations [11]. It also causes eye irritation, painful sensitization to light, and permanent injury to cornea and conjunctiva [9]. CV is a mitotic poisoning agent that is carcinogenic, considered as a potential biohazard [12], and banned in food industries by the European Union. However, it is still widely used in textile, and inkjet printing, due to its low cost and its peculiar color. Physical, chemical and biological techniques have been reported in the literature to study their efficiency in wastewater decolorization [13]. Dyes can be successfully removed by coagulation-flocculation [14,15]. However, this technique produces a huge amount of sludge, which makes its handling difficult and contributes significantly to disposal costs [16]. Photocatalysis has been used to degrade anionic and cationic dyes, using solar energy and different

* Corresponding author.
E-mail address: claudio.cecone@unito.it (C. Cecone).

https://doi.org/10.1016/j.reactfunctpolym.2023.105763
Received 10 August 2023; Received in revised form 23 October 2023; Accepted 25 October 2023
Available online 31 October 2023

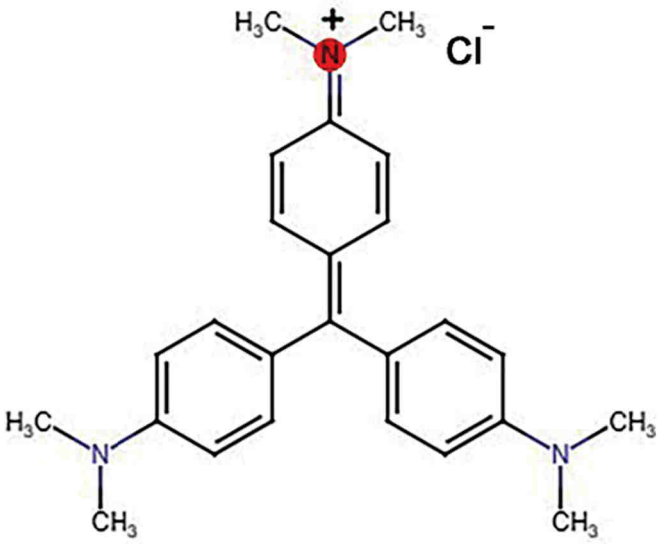

Fig. 1. Chemical structure of CV [10].

catalysts. They are often semiconductors activated by promotion of electrons from the valence band to the conductive band, and include Ag/ZnO thin films [17], magnetic TiO_2 [18] and bismuth titanate nanoparticles [19]. The weaknesses of this process, which limit their industrial applications, include low-usage of visible light, fast charge recombination, and low migration ability of the photo-generated electrons and holes [20]. Microorganisms such as bacteria, fungi, and yeasts have been found to efficiently decolorize various kinds of organic dyes present in wastewater [21]. Enzymes, like laccase have been widely used for the biological remediation of dyes, due to their abundance, affordable cost, and no requirement for additional chemical reagents [22,23].

The adsorption process is cost-effective, efficient, easy to implement at an industrial scale and the adsorbed dye can be recovered by regenerating the adsorption support [13]. Many materials have been tested to decolorize CV present in water, such as biopolymers [24], activated carbon prepared from biowastes [25,26], magnetic graphite composites [27], zeolite [28], chitosan [29], alginate [30] and electrospun fibers [31]. As for electrospinning, it is a promising technique, getting an increasing interest due to its simplicity, efficiency, low cost, and scalability [32]. The development of biobased fibers for the removal of organic dyes has become a major research topic in the last years [21]. Hosseini et al. (2021) prepared PVA (Polyvinyl Alcohol) /Chitosan/Montmorillonite fibers and evaluated their efficiency in the removal of cationic dye [33]. Kim et al. (2022) fabricated PVA/Lignin based fibers, showing high adsorption capacity toward methylene blue equal to 354 mg g^{-1} [34]. Polydopamine/β-cyclodextrin composite electrospun membranes have proven a good ability to remove cationic and anionic dyes from aqueous media [35]. Cellulose acetate fibers have been employed by Santos-Sauceda et al. (2021) for the decolorization of wastewater effluents [36]. These membranes have been prepared with biopolymers and stabilized by crosslinkers; however, this crosslinking is usually done using glutaraldehyde, which is classified as a carcinogen [37,38]. To overcome this issue, citric acid was used as green and eco-friendly crosslinker during the preparation of PVA based fibers [39–41]. Functionalization of PVA fibers has been reported in the literature, as a method to enhance their adsorption capacity for pollutants [42]. This step requires the use of additional reagents, that could be harmful and toxic to the environment such as, poly(hexadimethrine bromide) and poly(methyl methacrylate) [43], polyethyleneimine [44] and mercaptopropionic acid [45]. However, L-cysteine is a nontoxic amino acid and exhibits a simple molecular structure consisting of carboxylic (-COOH), amine (−NH2) and thiol (-SH) groups [46]. CYS emerges as an outstanding candidate for integrating into adsorbents designed for the removal of pollutants and few works have been reported on this topic. Enache et al. (2017) prepared CYS functionalized silica coated magnetite nanoparticles as potential adsorbent of Pb [47]. Mittal et al. (2021) synthesized a novel bio-nanocomposite Alginate-Cysteine-Kaolin for the effective removal of *CV* dye [48]. Moran-Salazar et al. (2023) have produced a novel L-cysteine-functionalized silica adsorbent designed for the removal of As(V) ions from aqueous solutions using a modified sol-gel route [49]. In this work, CYS offers two advantages due to the presence of the amino, carboxylic and thiol groups in its structure. It can bind to PVA through the formation of ester and amide bridges, ensuring thus the crosslinking of this polymer and it has also notable affinity to bind strongly to organic dyes.

Response surface methodology is a powerful statistical tool for modeling and optimizing complex processes in various fields, such as food science [50], biosensors [51], water treatment [52], agriculture [53], medicine [54] and drug delivery materials [55]. Doehlert experimental design is a second order polynomial model offering simultaneous study of multiple factors at different number of levels [56]. This model requires fewer number of experiments compared to other models (CCD, BBD), which is valuable when conducting costly or time-consuming experimental runs [57]. Doehlert matrix is characterized also by a uniform distribution of points over the whole experimental domain. In this context, this model has been employed to study the adsorption process of CV on PVA and PVA-CYS fibers.

In this work, green in-situ incorporation of L-cysteine into the PVA fibers has been performed in a single step by solubilizing the polymer, amino acid and crosslinker together and then proceeding with the electrospinning process. This procedure is quite easy, eco-friendly, and to the best of our knowledge, not well exploited in literature. The produced fibers were characterized by the determination of pH of Point Zero Charge (PZC), elemental analysis, Fourier Transform InfraRed spectroscopy (FTIR), Scanning Electron Microscopy (SEM), Atomic Force Microscopy (AFM), and thermogravimetric analysis (TGA). Experimental design approach has been applied to study the effects of each parameter and their interactions on the adsorption uptake of CV on both PVA and L-cysteine modified PVA, called PVA-CYS in this manuscript. The effect of water salinity has been investigated. CV removal mechanism was elucidated based on the characterization of Fourier transform infrared (FTIR), adsorption kinetics and isotherm models and the work were concluded with an application on a real effluent.

2. Materials and methods

2.1. Materials

Polyvinyl alcohol (PVA) with an average molecular weight of 89,000–98,000 Da (99% hydrolyzed), citric acid (99%), L-cysteine (CYS) (99%), sodium hydroxide, hydrochloric acid, sodium chloride (99%), were purchased from Sigma Aldrich. Sodium nitrate (99%), sodium sulfate (99%) and sodium carbonate (99%) were provided by Merck. Deionized water was used to prepare the solutions.

2.2. Fibers preparation

1 g of PVA has been dissolved in 10 mL of water at 85 °C. Then, 0.195 g of citric acid was added to the solution. For the preparation of PVA-CYS, after cooling to room temperature PVA blend, 0.3 g of CYS were introduced into the polymer mixture and stirred for 1 h to obtain a homogeneous solution. Prior to electrospinning, the mixture was sonicated for 30 min. The electrospinning set-up was self-made in laboratory and is composed of a volumetric pump, a power supply, and a rotary collector (Linari NanoTech Easy Drum, Pisa, Italy). The electrospinning process was performed using 30 kV field strength, 15 cm tip-to-collector distance (Speed: 75 rpm) and 0.9 mL h^{-1} flow rate. After electrospinning, the fibers were cured by thermal treatment at 180 °C for 30

min. Two types of fibers have been prepared during this work: PVA pure fibers and PVA-CYS fibers after addition of the amino acid to the mixture.

1.1. Characterization

The pH of zero charge (pH_{pzc}) of PVA and of PVA-CYS was determined using the procedure proposed by Faria et al. [58]: 30 mg of the material were introduced in six vials containing 10 mL of NaCl (0.01 mol L^{-1}) then the pH was adjusted in the range 2 to 12 with HCl or NaOH (0.1 and 1 mol L^{-1}). The mixtures were maintained under stirring for 24 h. Finally, the final pH was measured using pHmeter (Metrohm, Switzerland). The pH_{pzc} is the intersection point of the graph Initial pH-Final pH versus Initial pH with the x axis. Water solubility of the fibers was determined at room temperature according to the method mentioned by Cecone et al. [59] with slight modifications. Briefly, 20 mg of fibers was mixed with 5 mL of distilled water at room temperature for 24 h. Then, the mixture was centrifugated and the membrane was dried in the oven at 60 °C until it reached constant weight. The soluble fraction was calculated from the residue after evaporation using the following equation:

$$W_{loss}(\%) = \frac{(w_0 - w_1)}{w_0} \times 100$$

where, w_0 is the initial weight (mg) and w_1 is the final weight after drying (mg).

The chemical composition of the fibers (CHNS-O elemental analysis) before and after washing was measured using a Thermo Fisher FlashEA 1112 Series elemental analyzer (Waltham. MA. USA). A Perkin Elmer Spectrum 100 FTIR Spectrometer (Waltham, MA. USA) equipped with a universal ATR (Attenuated Total Reflection) sampling accessory was used for the recording of FTIR spectra. They were collected in the wavenumber range from 650 to 4000 cm^{-1}, with a resolution of 4 cm^{-1}. The morphology of the prepared materials was observed by SEM using Tescan VEGA 3 instrument (Brno. Czech Republic). The images were recorded using secondary electrons at 15 kV accelerating voltage. To reduce the sample charging, specimens were coated with gold before analysis using a Baltec SCD 050 sputter coater (Pfaffikon, Switzerland) operating under vacuum and at 60 mA. Nanosurf Easyscan2 AFM instrument shielded in an insulated enclosure and placed on an anti-vibration platform equipped with a high-resolution scan head (10 × 10 μm) was used to perform AFM analysis. Measurements were operated in air at room temperature in the intermittent-contact mode using a sharp Si cantilever 225 μm long (Tap190Al, BudgetSensors) with a tip height of 17 μm and an apex radius < 10 nm. AFM images of 256 × 256 lines were collected at 0.2–0.3 Hz scan rate. Thermogravimetric analysis was performed using TA Q500 instrument (New Castle, USA) to evaluate the thermal stability of the fibers. The initial sample weight was about 7 mg. Measurements were carried out in nitrogen atmosphere, at a temperature range of 30 to 650 °C, with a heating rate of 10 °C min^{-1}.

2.3. Adsorption experiments

The efficiency of PVA and PVA-CYS toward CV removal was evaluated by batch adsorption study. Kinetic studies were conducted at different times ranging from 15 to 180 min, with a CV concentration of 50 mg L^{-1}, pH equal to 5.88, 1 g L^{-1} fibers and stirred at 450 rpm (tested volume = 10 mL). The residual concentration of *CV* was determined using Varian Cary 300 Scan UV–Visible spectrophotometer measuring the absorption at 590 nm after removal of the fibers.

The removal percentage Y (%) and the adsorption capacity qe (mg g^{-1}) were calculated according to the equations:

$$Y = [(C_0 - C_e)/C_0] \times 100 \quad (1)$$

$$q_e = (C_0 - C_e) \times V/W \quad (2)$$

Table 1
Variables and experimental range of the Doehlert design.

Independent Variables		-1	0	+1
X1	Adsorbent amount (g L^{-1})	0.5	1	1.5
X2	pH	3	6.5	10
X3	Dye concentration (mg L^{-1})	50	100	150

where, C_0 (mg L^{-1}) is the initial concentration, C_e (mg L^{-1}) is the concentration at equilibrium, V (L) is the solution volume and W (g) is the adsorbent amount.

Adsorption isotherms were performed in the concentration range 50 to 250 mg L^{-1}, pH equal to 5.88, 1 g L^{-1} fibers and at room temperature. All presented data are done in triplicate and expressed as mean ± standard deviation (SD). Thermodynamic studies were carried out at pH equal to 5.88, 1 g L^{-1} fibers and four different temperatures (293, 303, 313, 323 K). The regeneration of PVA-CYS was tested by recovering the fibers after adsorption experiments and drying them overnight at 80 °C. Desorption experiments were conducted using four solvents: sodium hydroxide NaOH (0.1 mol L^{-1}), sodium chloride NaCl (0.1 mol L^{-1}), sodium hydrochloride HCl (0.1 mol L^{-1}) and distilled water. The regenerated fibers were washed several times with distilled water, dried and reused for further CV adsorption experiments.

2.4. Doehlert experimental design

Three factors Doehlert design was chosen to investigate effect and the interaction of the selected parameters on the removal percentage of CV. This model has the specificity of attributing different levels to each parameter and it is always recommended to select the variable with highest effect as the second factor, presenting seven levels [60]. Thus, seven levels were attributed to the variable pH (X2), five levels to the adsorbent amount (X1) and three levels to the dye concentration (X3) in the experimental range presented in Table 1. The required number of experiments for this design is equal to $k^2 + k + cp$, where k is the number of variables and cp is the number of replicates of the central point [61]. In our study, fifteen experiments have been carried out. Two responses (Y1 and Y2 were recorded for each experiment, corresponding to the adsorption capacity of CV on PVA and on PVA-CYS, respectively. The model was evaluated through Fischer's test, *p*-value and the coefficient of determination r^2. Nemrodw software was used to elaborate the statistical tests and 2D isoresponse graphs.

2.5. Effect of salinity

The effect of ionic strength has been tested using different concentrations of NaCl, from 0.01 to 0.4 mol L^{-1}. Moreover, to investigate the influence of coexisting ions, fibers were also added into 10 mL of 50 mg L^{-1} CV solution in the presence of 50 mg L^{-1} of SO_4^{2-}, NO_3^{2-} and CO_3^{2-}. The solutions were mixed and stirred at 450 rpm for 2 h.

2.6. CV adsorption in spiked real wastewater

CV was spiked in real wastewater at the concentration of 100 mg L^{-1}. Wastewater characterization was performed by inductively coupled plasma optical emission spectroscopy (ICP-OES) PerkinElmer, model Optima 7000 DV (Waltham, MA. USA) equipped by a Teflon Mira Mist nebulizer, a cyclonic spray chamber, and an Echelle monochromator. The applied power was 1300 W. Plasma, auxiliary, and nebulizer gas flows were 15, 0.2, and 0.6 L min^{-1}, respectively. The signals were measured in triplicate. The concentrations of K, Na, Ca, Mg, Sr, Si, Cr, Pb and Cd were measured at 766.490, 589.592, 317.933, 285.213, 407.771, 251.611, 267.716, 220.353 and 228.802 nm, respectively.

Table 2
Chemical properties of PVA and PVA-CYS.

	PVA	PVA-CYS	
pH of zero charge	4.48	4.16	
Soluble fraction (%)	0.70 ± 0.32	10.26 ± 3.08	
Elemental analysis		BW*	AW*
Carbon (%)	52.44 ± 0.12	50.24 ± 0.68	50.54 ± 0.72
Hydrogen (%)	8.10 ± 0.01	7.70 ± 0.15	7.89 ± 0.22
Oxygen (%) *	39.34 ± 0.12	36.96 ± 0.34	38.43 ± 0.38
Nitrogen (%)	0.00 ± 0.00	2.03 ± 0.10	1.35 ± 0.27
Sulfur (%)	0.00 ± 0.00	3.06 ± 0.17	1.79 ± 0.31

*BW: Before Washing. *AW: After Washing the fibers, * Oxygen (%): The oxygen content has been calculated by difference.

3. Results and discussions

3.1. Fiber characterization

Chemical properties of PVA and PVA-CYS fibers are summarized in Table 2. The pH of zero charge of the two fiber types was determined to be 4.48 and 4.16 for PVA and PVA-CYS, respectively, indicating the materials are negatively charged in a large range of pHs (i.e., for pHs > pH of zero charge). This parameter is crucial to understand the electrostatic interactions between the cationic dye and the charged surface of the fibers, depending on the solution pH [62]. Elemental analysis of PVA-CYS fibers shows the presence of nitrogen and sulfur (Table 2). This result confirms the effective functionalization of the amino acid within the PVA matrix [63] and is in accordance with FTIR absorption bands observed in Fig. 2 at 1650 and 1521 cm^{-1}, corresponding to C═O amide stretching vibration and N—H bending vibration, respectively [28,64]. After washing the PVA-CYS fibers, 90% of the starting material is recovered, which confirms the occurrence of the crosslinking reactions [59]. The weight loss of 10% is correlated to the decrease in the percentage of nitrogen and sulfur, as shown in Table 2, and can be associated to loss of unreacted amino acid not strictly bonded to the polymeric network. PVA fibers are stable in water and the soluble fraction is negligible.

Surface functional groups of CYS, pure PVA, crosslinked PVA fibers with citric acid (PVA-CA) and PVA-CYS were characterized by FTIR spectroscopy, as shown in Fig. 2. All the spectra show the specific

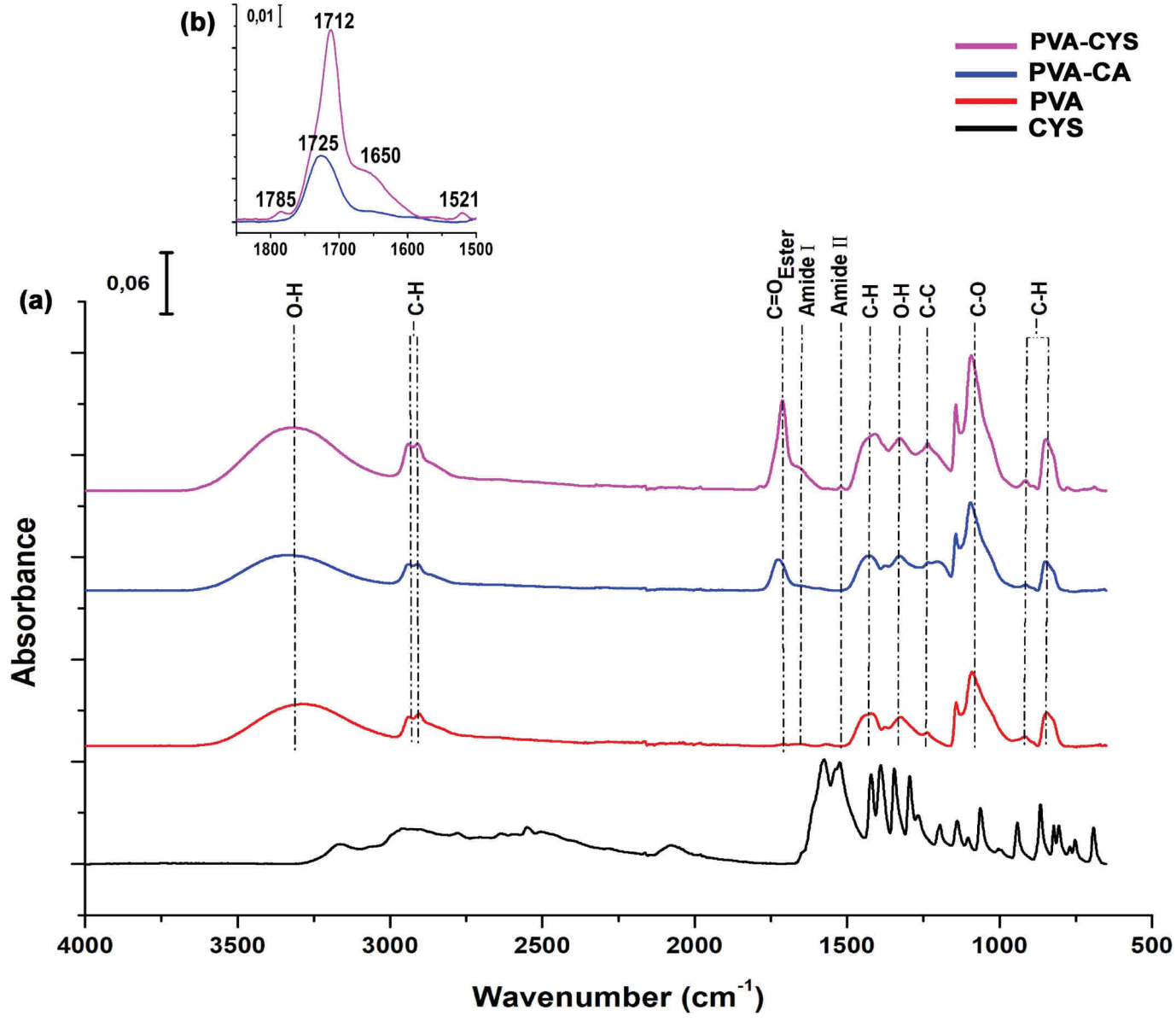

Fig. 2. FTIR Spectra of pure PVA, CYS, PVA-CA and PVA-CYS (a).

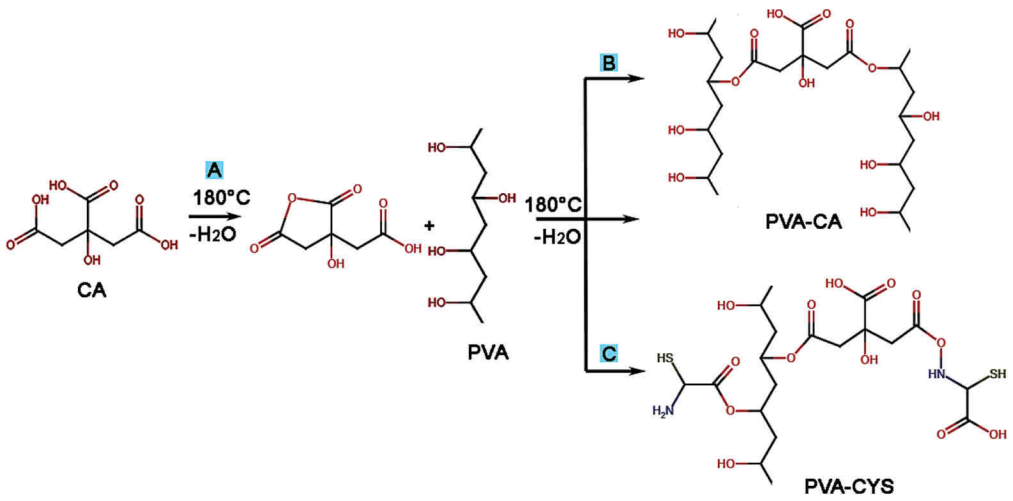

Fig. 3. Possible reactions between CA, CYS and PVA during the crosslinking treatment: (a) Formation of citric anhydride intermediate, (b) Ester bond formation during the crosslinking of PVA-CA and (c) Ester bonds formation as bridges between PVA and both CA and CYS and amide bonds between CA and CYS.

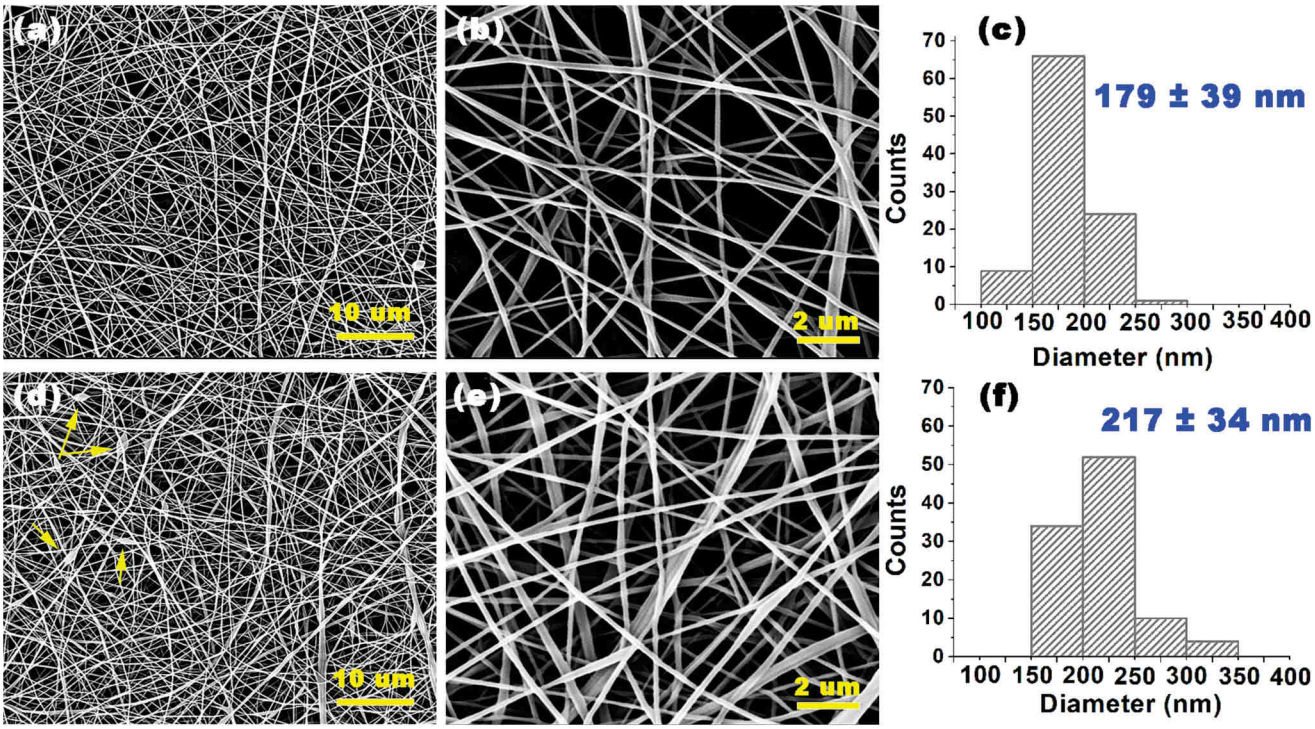

Fig. 4. SEM images of PVA (a, b), PVA-CYS (d, e), and Diameter size distribution of PVA (c) and PVA-CYS (f).

absorption bands of PVA: large O—H stretching band centered at 3285 cm^{-1} [65], C—O stretching of alcohols at 1090 cm^{-1} [66]. Symmetric, asymmetric stretching and bending vibrations of C—H are observed at 2937 cm^{-1}, 2900 cm^{-1} and 1427 cm^{-1}, respectively [67]. The signals observed at 832 cm^{-1}, 916 cm^{-1}, 1235 cm^{-1} and 1328 cm^{-1} are correlated to PVA skeleton vibrations: -CH_2 wagging and rocking, C—C stretching and O—H bending, respectively [8,9].

L-cysteine spectrum presents two characteristic peaks at 1579 cm^{-1} and 1421 cm^{-1} corresponding to the symmetric and asymmetric stretching vibrations of the COO^- group, respectively [70]. The bands appearing at 3168 $cm^{-1}$and 1533 cm^{-1} belong to the stretching and bending vibration of the amino group [71]. S—H bending vibration is observed at 2550 cm^{-1}.

The new band appearing at 1725 cm^{-1} in the PVA-CA fibers corresponds to the carbonyl of an ester group. The presence of this band confirms the reaction between hydroxyl groups of PVA and carboxylic groups of citric acid to form crosslinked PVA-CA fibers [41,72]. During the thermal process, CA is firstly dehydrated to its anhydride and subsequently an ester group is formed through ring opening reaction of the anhydride by the -OH groups of PVA (Fig. 3a and b) [73]. Hussein et al. indicated that CA could react with -OH of two separate PVA chains or with -OH of the same chain, forming intermolecular/intramolecular crosslinking [67]. After addition of L-cysteine, it is noticed that the carbonyl band signal shifts to lower wavenumber (1712 cm^{-1}). An increase in the hydrogen bonding interaction between the OH groups of PVA and the amino group of CYS may be responsible for this shift [74]. Compared with PVA-CA spectrum, two new absorption bands are observed at 1650 cm^{-1} and 1521 cm^{-1} in the PVA-CYS spectrum

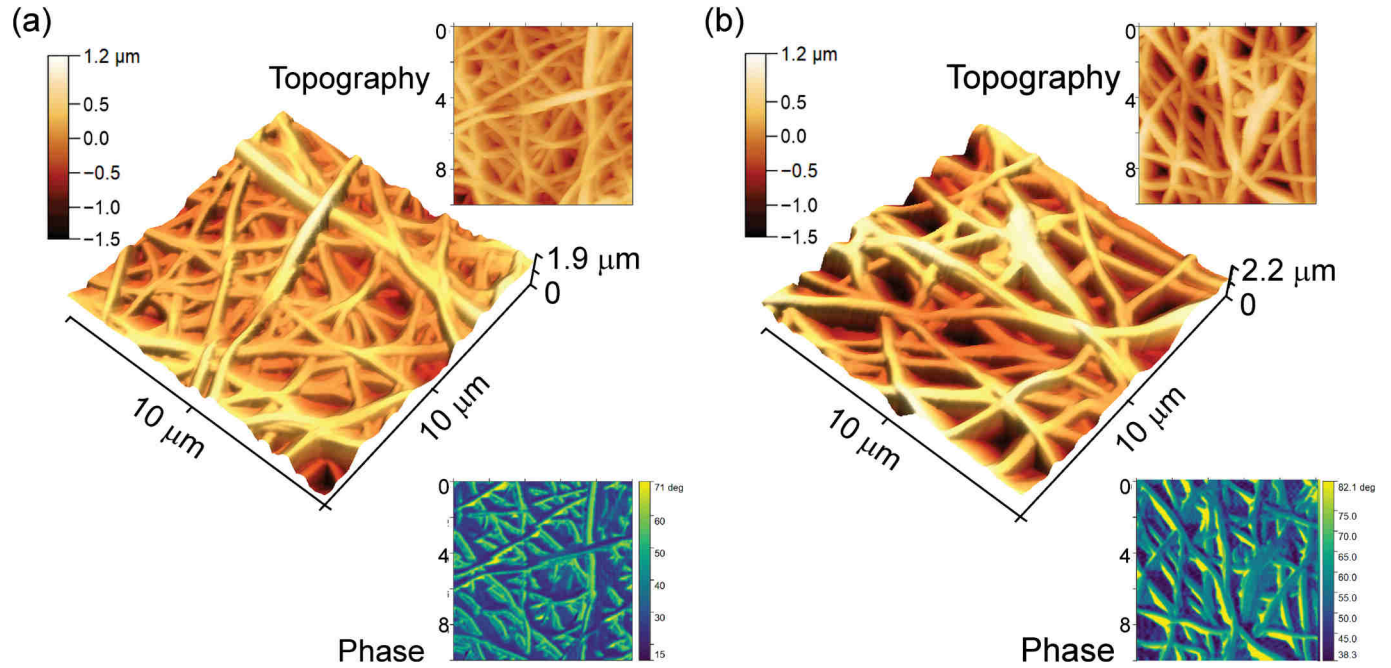

Fig. 5. 3D topography AFM images of: PVA (a) and PVA-CYS fibers (b). The top insets in (a,b) illustrate the 2D 10 × 10 µm top-view images, while the bottom insets in (a, b) show 2D phase signal images of the same regions.

(Fig. 2b). The first broad shoulder can be assigned to the amide I band [75], while the second small band belongs to amide II [64]. These observations confirm that the amino group of L-cysteine has reacted with the carboxylic group of citric acid during the crosslinking process of the PVA fibers, through the formation of amide groups (Fig. 3 b). Similar findings have been demonstrated by Urunga et al. during the synthesis of gelatin fibers crosslinked with citric acid [76].

Detail of the spectra in the range 1850–1500 cm^{-1} (b).

The morphology of the prepared fibers was studied via SEM technique and is illustrated in Fig. 4. PVA fibers are nonwoven, bead free, smooth and show an apparently uniform diameter, as observed by other authors [77,78]. SEM images of PVA-CYS (Fig. 4 d-e) show nonwoven and smooth fibers with the presence of beads in some regions. The formation of beads could be associated with the instability of the polymer solution jet due to solution viscosity, net charge density carried by the electrospinning jet and surface tension of the solution, as observed by some authors [79]. Diameter size distributions of PVA and PVA-CYS fibers are shown in Fig. 4 (c-f). The PVA fibers have a mean diameter of 179 ± 39 nm that increased to 217 ± 34 nm after the addition of L-cysteine.

The AFM imaging was performed for analyzing the surface morphology, composition, and roughness of the PVA-based fibers. AFM images of PVA and of PVA-CYS are illustrated in Fig. 5 (a-b), respectively. From the 3D images it is also clear that both PVA and PVA-CYS fibers are entangled and randomly distributed forming fiber mat membranes. Furthermore, it is also clear that PVA-CYS have bigger diameters than pure PVA fibers and that they present beads. Furthermore, from the phase signal of the two samples (insets at the bottom right of Fig. 5a,b) the contrast in the phase signal can be observed to be mainly influenced at this magnification by the morphology, with no significant substructure (i.e. domains are continuous along the fiber axis without interruptions) [80]. This finding indicated that the composition along the fiber axis at the surface is homogeneous and that there are no variations in surface properties, such as elasticity, adhesion and friction determined by the different composition and phases segregation [81].From the morphological signal of the two samples, root-mean-square roughness (R_{rms}) and mean roughness (R_a) [82] were calculated to be 162 nm and 130 nm for PVA, and 339 nm and 267 nm for PVA-CYS, respectively.

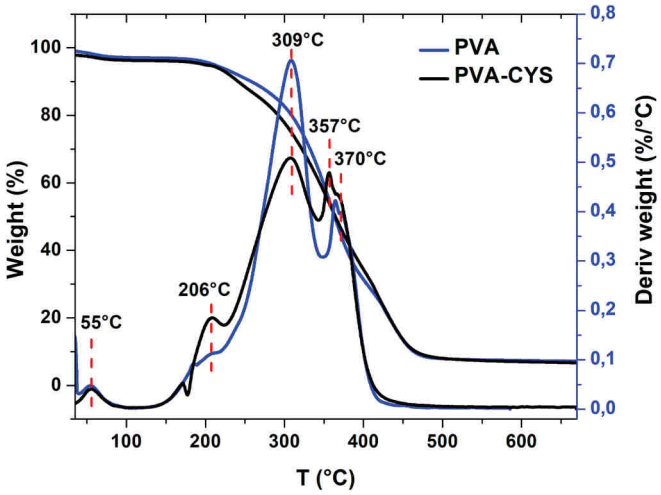

Fig. 6. TGA and DTGA thermograms of PVA and PVA-CYS.

The roughness values of samples were calculated after removal of highly curved/sloped surfaces of fibers and bottom mat regions (Fig. S2). From these results, we can state that the higher roughness values were calculated for fibers with larger diameters (i.e., PVA-CYS fibers), as observed by other authors for PLC fibers [83].

The thermal stability of PVA and PVA-CYS fibers was analyzed using TGA (Fig. 6). The profile of the curves presents four weight losses. The first one, observed at 55 °C, is related to the evaporation of adsorbed water [84]. Then, a second and a third weight losses between 200 and 310 °C can be assigned to the loss of side groups, namely the L-cysteine derivative in PVA-CYS and -OH by dehydration in PVA, with the formation of polyene [85,86]. A shift is also noticed in the following decomposition step, between 350 °C and 400 °C, corresponding to the cleavage of C—C in PVA main chain [87]. The different profiles of these steps can be ascribed to a different organization of the polymeric matrices and confirm the presence of cysteine in the modified membranes.

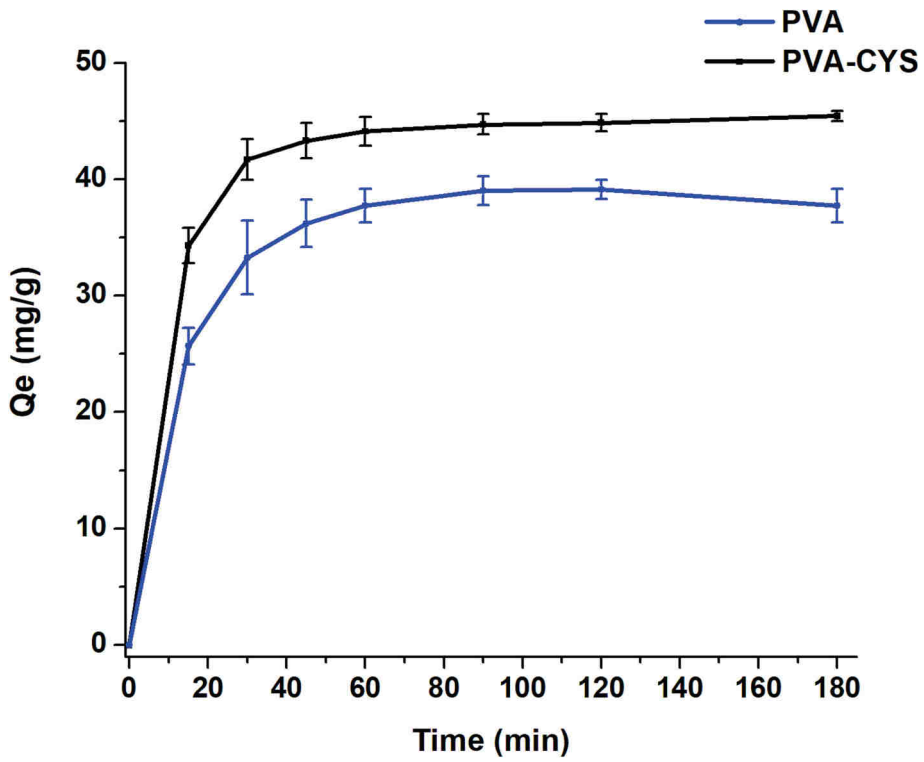

Fig. 7. Effect of contact time. Experimental conditions: 1 g L^{-1} fibers, pH = 5.88, and 50 mg L^{-1} CV.

Table 3
Matrix of experiments and recorded responses.

Run	X1	X2	X3	Y1	Y2
1	1.50	6.50	100.00	31.73	59.25
2	0.50	6.50	100.00	35.43	134.41
3	1.30	10.00	100.00	80.77	58.22
4	0.80	3.00	100.00	10.29	70.77
5	1.30	3.00	100.00	11.08	58.05
6	0.80	10.00	100.00	123.72	86.86
7	1.30	7.67	150.00	41.27	89.95
8	0.80	5.33	50.00	36.19	73.83
9	1.30	5.33	50.00	29.86	48.71
10	1.00	8.83	50.00	62.73	59.91
11	0.80	7.67	150.00	64.92	134.55
12	1.00	4.17	150.00	29.83	95.46
13	1.00	6.50	100.00	33.48	81.82
14	1.00	6.50	100.00	33.01	83.06
15	1.00	6.50	100.00	32.39	79.39

3.2. Application of Doehlert experimental design

Before performing the adsorption experiments of the experimental design, it was necessary to investigate the kinetics of adsorption, to determine the time required to reach the adsorption equilibrium (Fig. 7). The graph shows rapid adsorption in the first 30 min, then the rate slows down, and equilibrium is reached after approximately 2 h, indicating saturation of the active sites. The time of two hours was considered for the rest of the experiments carried out.

The response values obtained for each experiment are listed in Table 3. The adsorption capacities of CV ranged from 10.29 to 123.72 mg g^{-1} and 48.71 to 134.41 mg g^{-1} for PVA and PVA-CYS, respectively. The Fischer test was applied to evaluate the significance of the model (Table S1). The *p* values of the two models are <0.001 and 0.01 for CV adsorption on PVA and PVA-CYS, respectively. The coefficients of determination are equal to 0.946 and 0.976 for Y1 and Y2, respectively. These results prove a good and satisfactory correlation between the experimental and predicted responses.

The Doehlert design is a second order model, relating the studied responses to the variables amount, pH and concentration of the dye, through the following equations:

$$Y1 = 33.40 - 10.21 \times {}_1 + 47.33 \times {}_2 + 0.93 \times {}_3 + 31.06 \times {}^2_2 + 8.58 \times {}^2_3 - 24.67 \times {}_1 \times {}_2 + 6.09 \times {}_2 \times {}_3.$$

$$Y2 = 81.42 - 32.67 \times {}_1 + 5.75 \times {}_2 + 28.06 \times {}_3 + 15.40 \times {}^2_1 - 22.40 \times {}^2_2 - 9.19 \times {}_1 \times {}_2.$$

Pareto chart is principally used to identify the factors and interaction effects that have the most impact on the adsorption process (Fig. 8) [88]. The length of each bar in the diagram represents the influence of the parameter. Fig. 8 (a) shows for PVA that pH (X2) is the most influencing factor on the CV adsorption capacity with an effect percentage >50% followed by the interaction between adsorbent amount (X1) and pH in much more limited way. However, Fig. 8 (b) revealed that the adsorbent amount (X1) and the initial dye concentration (X3) have the higher percentage of effect on CV adsorption on PVC-CYS followed by the pH (X2) in a much more limited way.

The isoresponse graphs were obtained using the Nemrodw software. The model equation is basically transformed into isoresponse curves for the purpose of the model's graphical evaluation [89]. The study of the influence of different parameters on the adsorption capacity of CV was performed by varying two factors and fixing the third one. These plots are presented in Figs. 9-11.

as a function of adsorbent amount and pH at constant dye concentration (100 mg L^{-1}).

The solution pH is a very important factor in the adsorption process of CV dye. Adsorbent and adsorbate may include functional groups that can be protonated or deprotonated to generate different surface charges in solution, depending on pH, leading to electrostatic attraction or repulsion between the charged adsorbate and adsorbent [90]. Therefore, pH was investigated in the range of 3 to 10 to study its impact on the CV dye removal on PVA and PVA-CYS. As shown in Fig. 9 (a), a significant improvement in the adsorption capacity of CV on PVA is observed as pH increases. In fact, at high pH values, CV dye is almost totally positively charged [91,92], whereas the fibers are negatively charged as the pH is

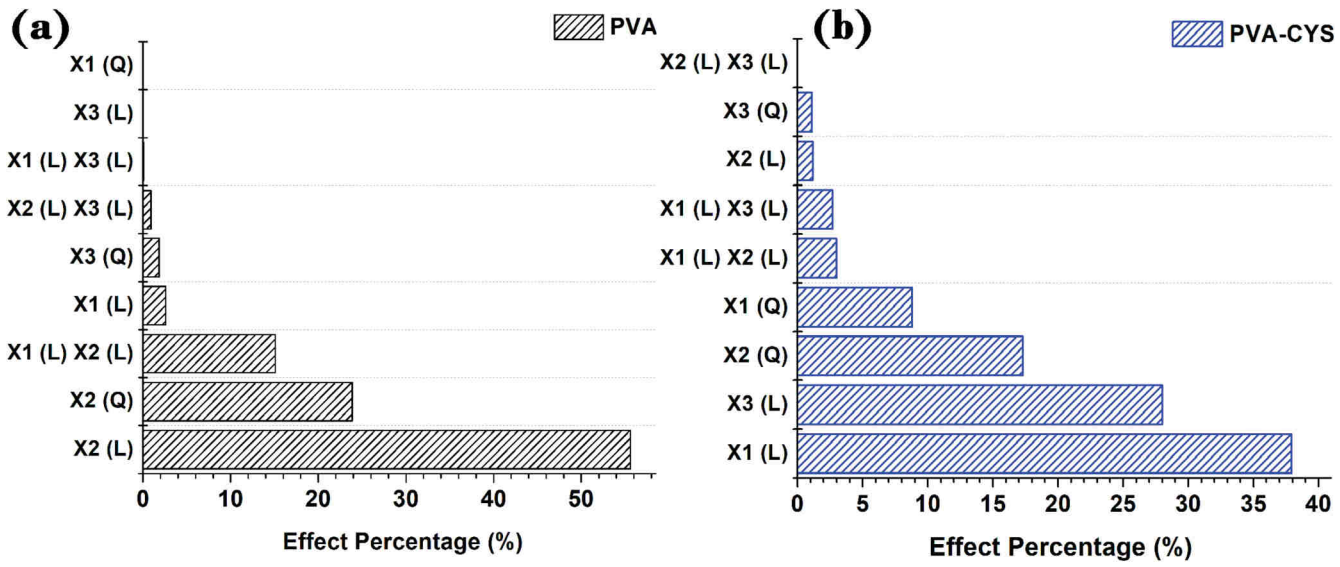

Fig. 8. Pareto Graph for CV adsorption capacity on PVA (a) and PVA-CYS (b).

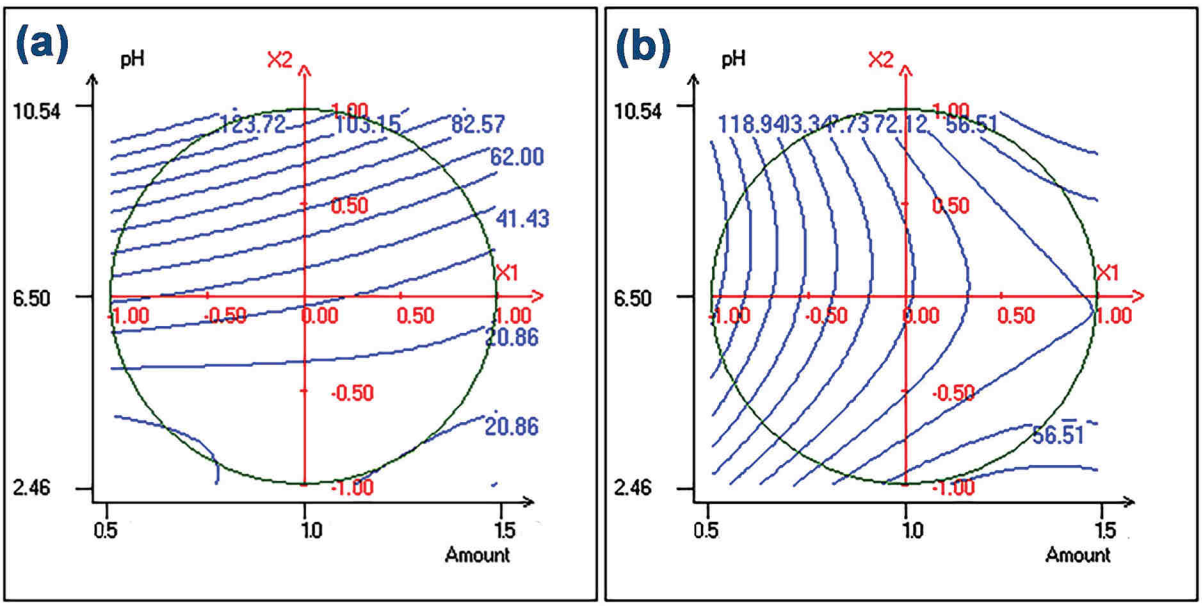

Fig. 9. Contour plots of CV adsorption capacity on PVA (a) and PVA-CYS (b).

higher than the pH of the zero charge (equal to 4.48). In this condition, an electrostatic attraction between the cationic dye ions and the negatively charged fiber surface takes place, which enhances the removal of CV dye. By contrast, at pH solution lower than pH of zero charge, there is an electrostatic repulsion between the CV cations and the positively charged surface of the fiber [93]. Furthermore, in acidic media the adsorption capacity decreases due to the large concentration of H^+ ions, which compete with the positively charged CV molecules for the adsorption on the fibers, resulting in lower CV adsorption capacity on PVA [94]. The maximum adsorption capacity of CV on PVA reached 114 mg g^{-1} at pH 10 and 0.75 g L^{-1} of adsorbent amount (Fig. 9 a).

Fig. 9 (b) shows the effect of pH and adsorbent amount on CV adsorption by PVA-CYS. It is observed that pH variation affects differently the removal uptake of CV on PVA-CYS compared to PVA. This difference lies in the incorporation of cysteine, introducing novel functional groups like NH_2 and SH groups onto the modified fibers. The results have shown that at acidic pH, CV uptake decreases for PVA due to the electrostatic repulsions between cationic dye and negatively charged surface of PVA. However, the CV adsorption capacity remains high for PVA-CYS even in acidic media. The amino and sulfur group of CYS can interact with CV molecules not only via electrostatic forces but also through hydrogen bonding, dipole-dipole, and hydrophobic interactions. The involvement of these various mechanisms is responsible for enhancing the dye removal efficiency at lower pH compared to PVA. These findings confirm that the adsorption mechanism did not include only electrostatic interactions but also physical and/or chemical interactions established between the dye molecule and the polymeric matrix. The use of PVA-CYS as an adsorbent has an effective capacity for dye removal at a close to neutral pH, which is also the natural pH of CV solution [91]. This outcome is important for the large-scale use of the adsorption process since it will not require any pH adjustment of the effluent prior to treatment.

The isoresponse curves of CV adsorption capacity as a function of initial concentration and amount of PVA and PVA-CYS are presented in

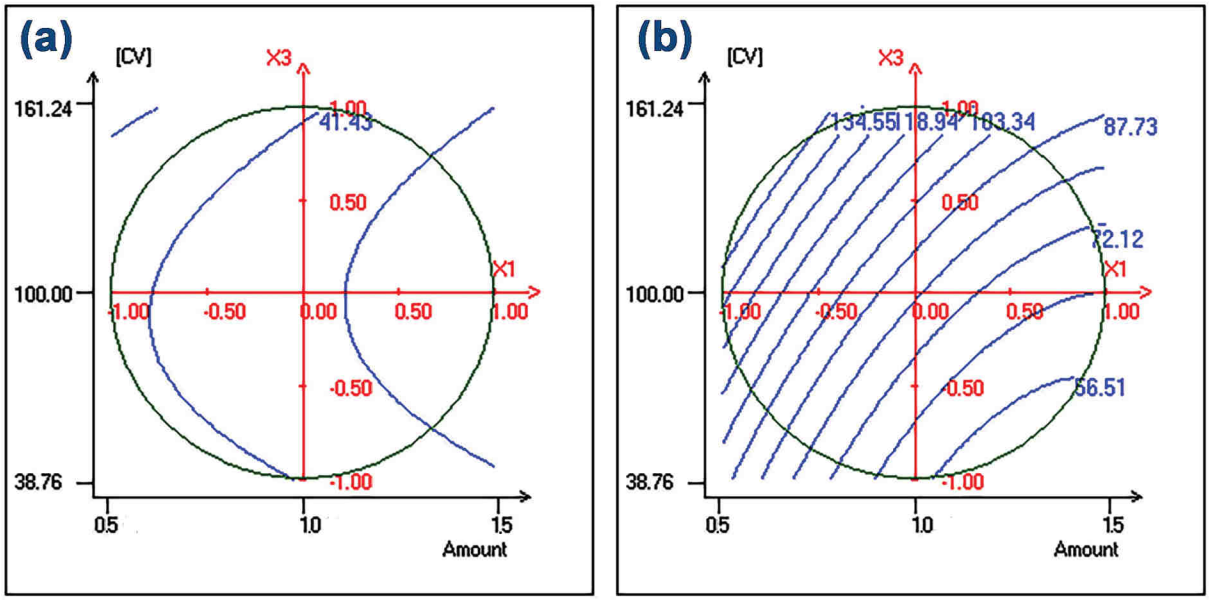

Fig. 10. Contour plots of CV adsorption capacity on PVA (a) and PVA-CYS (b) as function of adsorbent amount and dye concentration at constant pH (6.5).

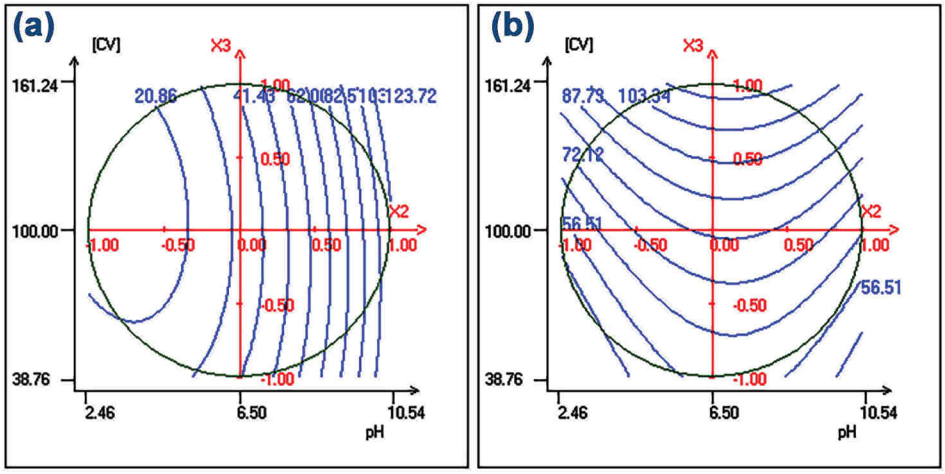

Fig. 11. Contour plots of CV adsorption capacity on PVA (a) and PVA-CYS (b).

Fig. 10 (a, b). The results show that with an increase in both fiber quantities, the adsorption capacity of CV dye decreases. When the amount of PVA increases from 0.5 to 1.0 g L^{-1}, the adsorption capacity decreases from 41.23 to 30.95 mg g^{-1} (Fig. 10 a). Similarly, the capacity decreases from 134.55 to 56.59 mg g^{-1} when the PVC-CYS amount increases from 0.5 to 1.0 g L^{-1} (Fig. 10 b).

Fig. 11 shows the effect of initial dye concentration and pH on adsorption capacity of CV on PVA and PVA-CYS. Adsorption capacity of CV increased with the initial concentration at all pH values for PVA-CYS (Fig. 11 b). Higher concentrations enhance the mass gradient between the dye solution and the fibers, which subsequently acts as a driving force for the transfer of dye molecules from the bulk solution to the fiber surface, leading to a higher CV uptake on PVA-CYS [95]. These graphs show better adsorption on highly basic media for PVA and in neutral media for PVA-CYS. These observations are in agreement with those reported previously for the effect of pH on CV adsorption capacity (Fig. 9).

as a function of dye concentration and pH at a constant amount (1 g L^{-1}).

3.3. Effect of salinity

The effect of solution ionic strength (i.e., salinity) was evaluated by the addition of different concentrations of sodium chloride, as shown in Fig. 12. The increase in ionic strength has a negative effect on the adsorption capacity of CV on PVA fibers, which decreases from 58 to 46 mg g^{-1}. This effect confirms that electrostatic attraction between the cationic dye and the fibers controls the adsorption process [96,97]. However, a slight increase in the adsorption capacity from 66 to 70 mg g^{-1} is observed for PVA-CYS fibers, indicating that the adsorption of CV is not affected by the solute ionic strength which confirms the results already discussed during the study of pH effect (Fig. 9.b). Therefore, the electrostatic interaction is not the main mechanism of CV adsorption on PVA-CYS fibers. Similar results have been obtained by Tran et al. during the adsorption study of cationic dye methylene green on biochar [98].

Fig. 13 presents the effect of nitrate and sulfate ions on CV removal by adsorption on PVA and PVA-CYS. The presence of nitrate does not affect the adsorption capacity of the dye for both fibers, whereas only a slight decrease of 5% was observed for PVA and PVA-CYS fibers when the sulfate ions were added. These results prove that PVA-CYS have an

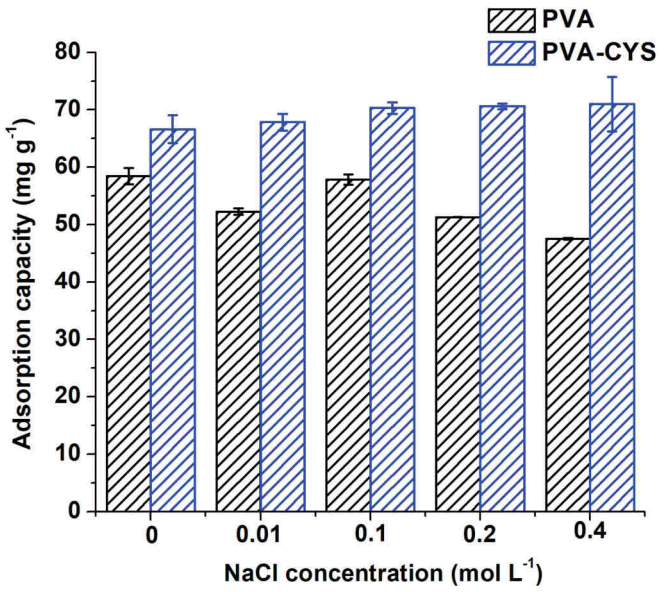

Fig. 12. Effect of ionic strength. Experimental conditions: 1 g L^{-1} fibers, pH 5.88, 2 h of adsorption, and 100 mg L^{-1} CV.

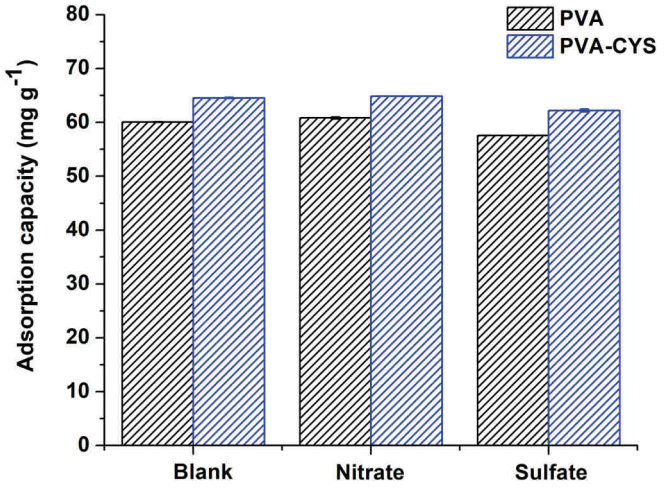

Fig. 13. Effect nitrate and sulfate ions on CV removal by PVA and PVA-CYS fibers. Experimental conditions: 1 g L^{-1} fibers, pH 5.94, 2 h of adsorption, 50 mg L^{-1} CV, and 50 mg L^{-1} of SO_4^{2-} and NO_3^-.

excellent selectivity toward CV. On the contrary, the study of CV removal in the presence of carbonate was affected by a problem that made impossible a good evaluation of the fibers adsorbing properties: the CV solution color changed from purple to green yellowish with modification of the absorption spectrum profile.

3.4. Adsorption Kinetics

Describing adsorption kinetics is essential for determining the rate of solute uptake. To fit the experimental data, three kinetic models were applied: Pseudo-first order and Pseudo-second order and Elovich model. They are expressed in the three following equations, respectively [99].

$$q_t = q_e\left(1 - e^{-k_1 t}\right) \quad (3)$$

$$q_t = \frac{k_2 q_e^{\,2}\, t}{1 + q_e k_2\, t} \quad (4)$$

$$q_t = A + B\, ln(t) \quad (5)$$

where, q_t and q_e are the adsorption capacity at time t and at equilibrium, respectively (mg g^{-1}), k_1 is the rate constant of pseudo-first-order model (min^{-1}), k_2 is the rate constant of pseudo-second-order model (min-1), A (mg g^{-1} min^{-1}) and B (g mg^{-1}) are the Elovich constants.

Fig. 14 shows the nonlinear fitting for the three models and Table 4 summarizes the kinetic parameters of each model. The pseudo-first-order kinetic model is the most appropriate for describing the adsorption of CV dye on both PVA and PVA-CYS, as it exhibits the highest correlation coefficient (R^2) and the lowest chi-square (χ^2) value among the models considered. The calculated equilibrium adsorption uptake q_e (cal) obtained from the fitting results are in agreement with the experimental value q_e (exp) for the pseudo first order model, as shown in Table 3. This model suggests that the adsorption occurs through physical forces between the solute molecules and the adsorbent surface.

3.5. Adsorption isotherms

The Langmuir and Freundlich models were used to evaluate the adsorption isotherms, and they are expressed in the following nonlinear forms, respectively [100]:

$$q_e = \frac{q_m K_L C_e}{1 + K_L C_e} \quad (6)$$

$$q_e = K_F C_e^{\,1/n} \quad (7)$$

where q_e (mg g^{-1}) and q_m (mg g^{-1}) are the equilibrium and maximum adsorption capacities of CV on the fibers, respectively; C_e (mg L^{-1}) is the equilibrium concentration; K_L is the Langmuir constant (L g^{-1}); K_F is the Freundlich constant (mg g^{-1}). (L $mg^{-1})^{1/n}$ and n is the heterogeneity factor.

The non-linear fitting plots of the two models are represented in Fig. 15 and the corresponding parameters are summarized in Table 5. Experimental data of the two systems are better fitted by Freundlich model that takes into account that the adsorption has not reached the saturation yet, nevertheless Langmuir monolayer capacity will be considered to give a more precise, although underestimated, comparison between the adsorption capacity of the two systems. The Langmuir maximum adsorption capacity of CV has increased from 89.68 mg g^{-1} to 197.21 mg g^{-1} after incorporating L-cysteine in PVA fibers. This enhancement with more than the double confirms the valuable role of the amino acid in increasing the interaction between the dye and fibers. Table 6 presents a comparison of the efficiency of PVA and PVA-CYS with other adsorbents reported in previous studies. Gellan gum/bacterial cellulose hydrogel [101], functionalized chitosan [102], and activated carbon [103] show maximum adsorption capacities of CV lower than 100 mg g^{-1}. However, PVA-CYS fibers show excellent adsorption capacity reaching 197 mg g^{-1}, due to the existence of different functional groups after addition of L-cysteine. The physical form of the adsorbents points out the positive aspect of an easy recovery of the electrospun fibers, prepared in this work, with respect to other dispersed systems.

3.6. Thermodynamic studies

The effect of temperature on the removal efficiency of CV on PVA-CYS was investigated at four different temperatures (293, 313, 323, 333 K). The thermodynamic parameters consisting of Gibbs free energy (ΔG_T°), enthalpy (ΔH_T°), and entropy (ΔS_T°) were calculated using the following equations:

$$\Delta G_T^\circ = -R\,T\,ln(K_c) \quad (8)$$

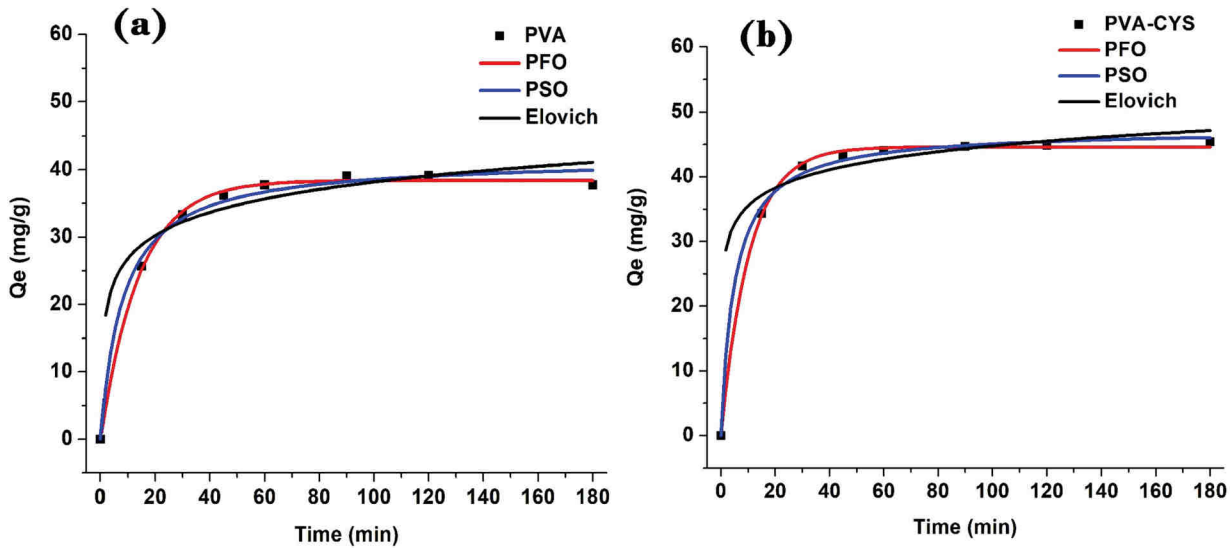

Fig. 14. Kinetics models for CV adsorption on PVA (a) and PVA-CYS (b). (Experimental conditions: 1 g L^{-1} fibers, pH = 5.88, and 50 mg L^{-1} CV).

Table 4
Kinetic parameters.

Model	Parameters	PVA	PVA-CYS
Pseudo First order	q_e (exp) (mg g^{-1})	37.738	44.850
	q_e (cal) (mg g^{-1})	38.402	44.611
	k_1 (min^{-1})	0.070	0.095
	R_2	0.998	0.999
	χ_2	0.407	0.269
Pseudo second order	q_e (exp) (mg g^{-1})	37.738	44.850
	q_e (cal) (mg g^{-1})	41.729	47.336
	k_1 (min^{-1})	0.002	0.004
	R_2	0.991	0.997
	χ_2	1.528	0.679
Elovich	A (mg g^{-1} min^{-1})	15.469	26.261
	B (g mg^{-1})	4.932	4.022
	R_2	0.969	0.986
	χ_2	5.362	3.260

$$\ln K_c = \frac{\Delta S_T^\circ}{R} - \frac{\Delta H_T^\circ}{R\,T} \quad (9)$$

$$K_c = \frac{C_0 - C_e}{C_e} \quad (10)$$

where, T is the temperature (K), R is the universal gas constant (8.314 J mol^{-1} K^{-1}), K_c is the coefficient of distribution, C_0 is the initial concentration (mg L^{-1}), and C_e is the concentration at equilibrium (mg L^{-1}).

Table 5
Parameters of Langmuir and Freundlich models for CV adsorption on PVA and PVA-CYS.

Fibers	Langmuir model			Freundlich model		
	q_m (mg g^{-1})	K_L (L g^{-1})	r^2	K_F (mg g^{-1}). (L $mg^{-1})^{1/n}$	n	r^2
PVA	89.68 ± 3.72	0.67 ± 0.21	0.831	48.18 ± 3.25	8.07 ± 0.93	0.943
PVA-CYS	197.21 ± 13.71	0.51 ± 0.24	0.779	78.52 ± 7.37	5.38 ± 0.56	0.961

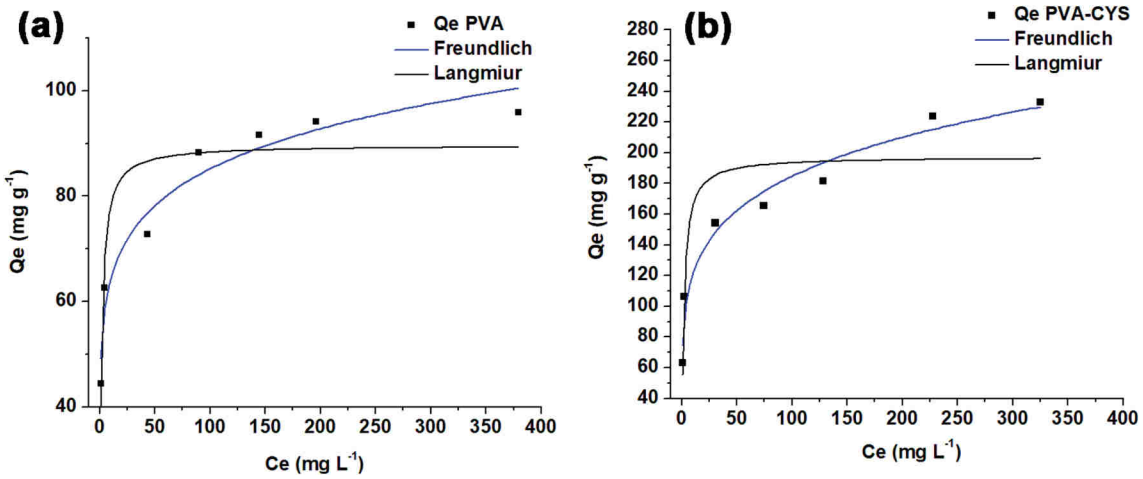

Fig. 15. Adsorption isotherms of CV on PVA (a) and PVA-CYS (b) Experimental conditions: 1 g L^{-1} fibers, pH 5.85, 2 h of adsorption.

Table 6
Comparison of the efficiency of PVA-CYS to other adsorbents reported in previous studies.

Adsorbent	Q_{max} (mg g^{-1})	Physical form	Ref
Gellan gum/bacterial cellulose hydrogel	13.49	Hydrogel	[101]
Functionalized chitosan	37.03	Powder	[102]
Activated carbon/Fe_3O_4 magnetic nanocomposite	35.30	Powder	[25]
Activated carbon	61.57	Powder	[103]
Polyacrylamide grafted *Actinidia deliciosa* peels	75.188	Powder	[104]
Alginate@silver nanoparticles bionanocomposite	186.93	Powder	[99]
Alginate-whey	220.00	Beads	[30]
Chitosan-modified l-cysteine/bentonite bionanocomposite	240.00	Powder	[105]
Microporous silica	250.00	Powder	[106]
$ZnCl_2$ activated cocoa leaves	253.30	Powder	[7]
PVA	89.68	Membrane	This work
PVA-CYS	197.21		

Table 7
Thermodynamic parameters of CV dye adsorption on PVA-CYS.

Temperature (K)	Q (mg g^{-1})	ΔG_T° (kJ mol^{-1})	ΔH_T° (kJ mol^{-1})	ΔS_T° (kJ K^{-1} mol^{-1})
293	68.320	−1.334	10.834	0.039
313	74.740	−2.196		
323	77.000	−2.542		
333	79.940	−2.873		

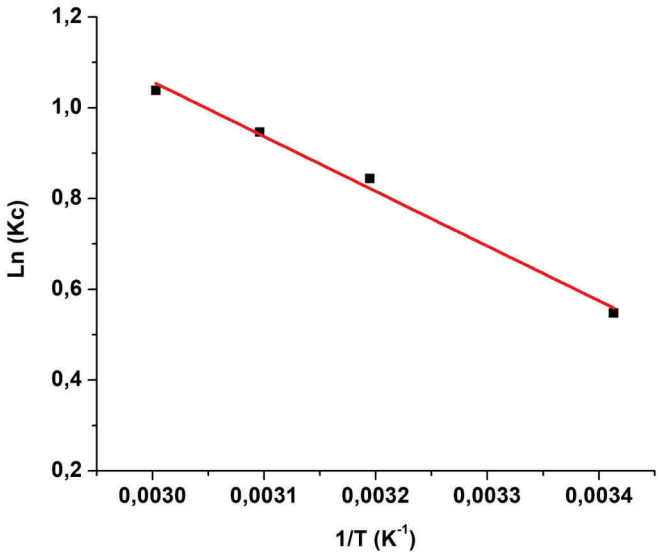

Fig. 16. Van't Hoff plot for CV adsorption on PVA-CYS.
(Experimental conditions: 1 g L^{-1} fibers, pH = 5.88, and 100 mg L^{-1} CV).

Temperature plays a crucial role in controlling the strength of adsorptive forces between the adsorbent and dye molecules [107]. The adsorption capacity of CV on PVA-CYS increased from 68.32 to 79.94 mg g^{-1} as the temperature rose from 293 K to 333 K, as shown in Table 7. The findings indicate that the adsorption process of CV is endothermic, implying that rising temperature would enhance the energy and promote the adsorption process. Bibi et al. 2023 reported similar findings while removing CV by adsorption on microalgae from real wastewater [108]. The values of thermodynamic parameters can be directly obtained from the slope and intercept of the van't Hoff plot (Fig. 16), and they are summarized in Table 7. The negative values of

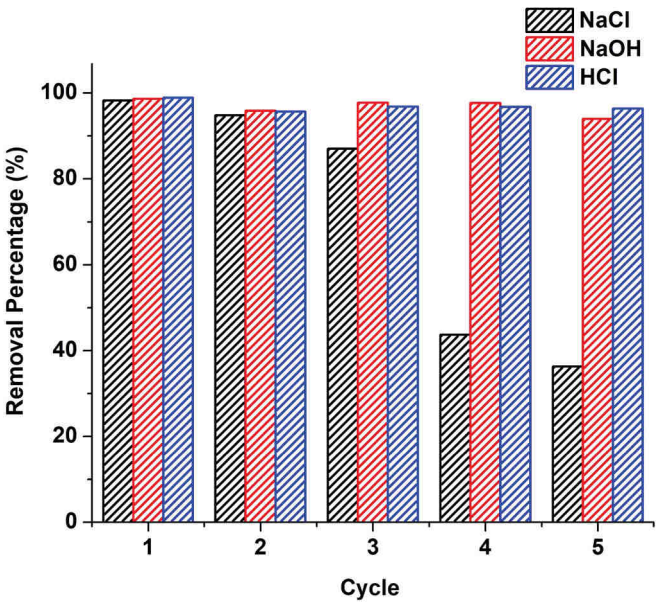

Fig. 17. Regeneration of PVA-CYS.

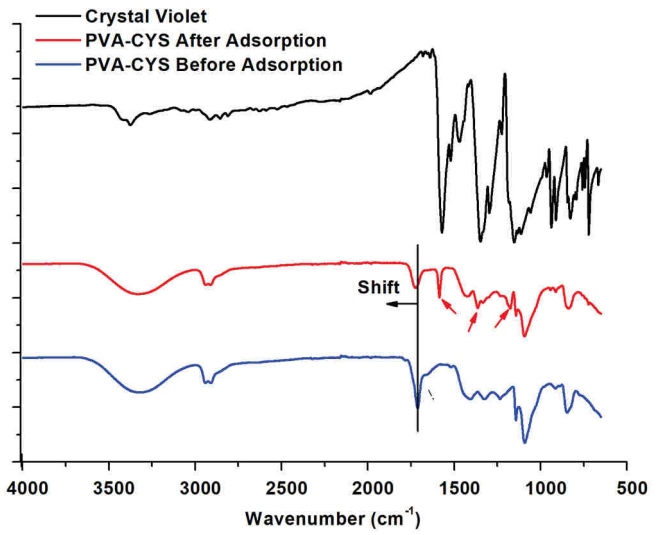

Fig. 18. FTIR spectra of pure CV, PVA-CYS before and after adsorption of CV.

Gibbs free energy at all temperatures reveals that the adsorption process is spontaneous and favorable [109]. The positive value of ΔH_T° indicates the endothermic aspect of the adsorption. The low value of enthalpy suggests the involvement of physisorption in CV adsorption on PVA-CYS [110]. The positive value of entropy demonstrates an enhancement in the randomness between the solid and the liquid interface.

3.7. Regeneration of PVA-CYS

Regenerating the used material is essential for assessing the economic viability and sustainability of the adsorption process. The desorption and reuse of PVA-CYS fibers were evaluated using four solvents H_2O, NaCl (0.1 mol L^{-1}), NaOH (0.1 mol L^{-1}) and HCl (0.1 mol L^{-1}). Fig. 17 presents the evolution of the CV removal percentage after 5 regeneration cycles. Water was excluded from subsequent regenerations due to an uptake lower than 30% after just one cycle. After five cycles of desorption using NaOH and HCl, the removal percentage of CV remains above 95%. However, NaCl did not desorb CV successfully with a

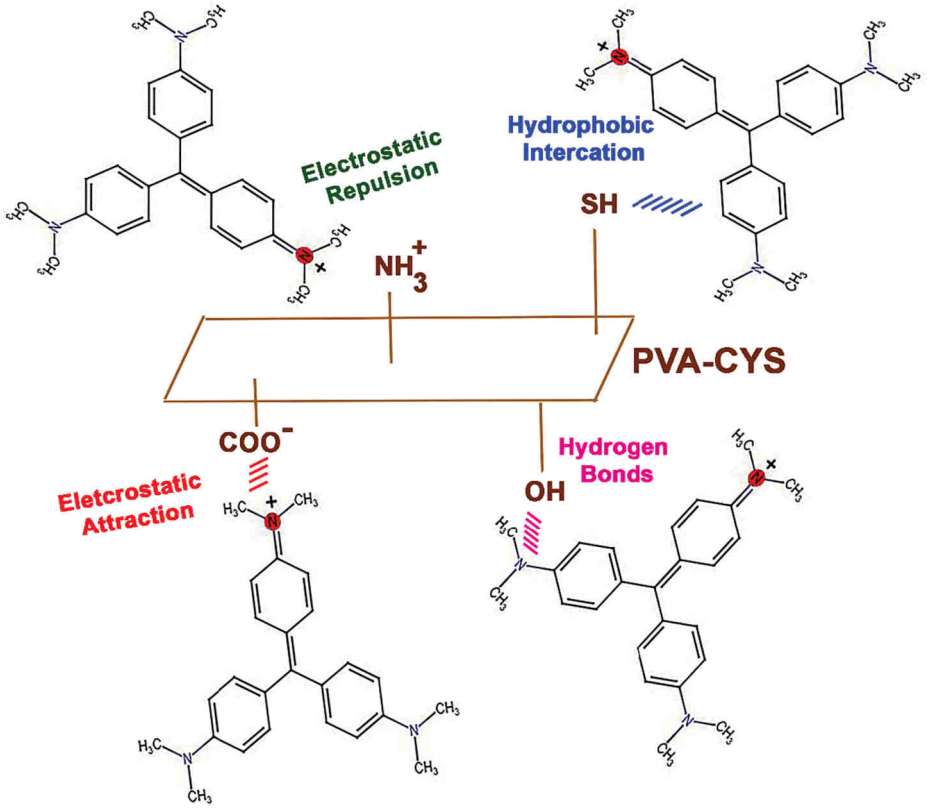

Fig. 19. Possible interactions between CV and PVA-CYS fibers.

decrease in the removal uptake from 96% of 36% after 5 cycles. Mirza et al. (2020) have found that 82% of CV could be desorbed from Alginate/pectin nanocomposite using HCl as desorbing agent [12]. These observations underscore the efficiency of PVA-CYS fibers for CV adsorption, coupled with their outstanding regeneration capabilities.

3.8. Adsorption mechanism of CV on PVA-CYS fibers

The adsorption mechanism of CV was hypothesized considering the FTIR spectra presented in Fig. 18, the pH of zero charge of the adsorbent and the effect of pH on the removal uptake of the dye, reported in Fig. 19. The pH of zero charge of PVA-CYS fibers was equal to 4.16, with respect to which higher pH values create a positively charged surface and lower pH values create a negatively charged surface [101]. CV is a cationic dye, and its adsorption should be enhanced by the electrostatic interaction with negatively charged fibers at pH >4.16. However, Fig. 9 b shows that the uptake of CV is less affected by the solution pH, compared to PVA and the adsorption capacities remain relatively high when the pH changes. This result proves that the adsorption mechanism cannot be mainly attributed to electrostatic interactions, hence hydrogen bonds between tertiary amino groups of CV and hydroxyl groups of PVA should be taken into account [102]. Fig. 18 presents the FTIR spectra of CV, PVA-CYS before and after adsorption. Absorption bands, indicated in the figure by red arrows, appeared in the FTIR spectrum after CV adsorption at 1585, 1365 and 1180 cm^{-1}: they are correlated to C═C stretching vibration of benzene ring, C—N stretching of aromatic tertiary amine and N-CH_3 stretching, respectively, and are characteristic of CV vibrations [111,112]. Their presence in the spectrum is a proof of the dye adsorption on PVA-CYS. Also, a shift in the absorption band of ester carbonyl group from 1712 to 1724 cm^{-1} is observed for PVA-CYS after adsorption, confirming an interaction involving the ester group has been established with CV molecule [113]. In addition, as Cysteine is considered an almost hydrophobic amino acid, an interaction involving the hydrophobic part of the amino acid and the aromatic rings of CV, is also possible [114]. This complex situation has been summarized in the scheme reported in Fig. 19, from which we can evidence an additional point: CV possesses three tertiary amino groups that can interact at the same time with at least three OH groups of PVA chains. If structural factors block the PVA chains and hamper their winding, as expected in the electrospun fibers, it is possible that one molecule of CV could interact with more than one polymeric chain causing a decrease of the efficiency of the adsorption increasing the amount of the adsorbent, as indicated by the experimental design results.

Table 8
Application on real effluent.

Parameter	Before treatment	After treatment
pH	8.34	7.94
Na (mg L^{-1})	91.48	85.17
K (mg L^{-1})	16.54	15.56
Mg (mg L^{-1})	31.95	28.65
Ca (mg L^{-1})	85.43	75.52
Cr, Pb, Cd	≤ LD	≤ LD
Sr (mg L^{-1})	0.86	0.79
Si (mg L^{-1})	9.17	7.02
CV (mg L^{-1})	108.43	17.12

3.9. Treatment of real effluent

The effectiveness of the process of CV adsorption has been assessed through the application of the PVA-CYS fibers as an adsorbent on a real effluent spiked with CV. The effluent was characterized by determining its pH, ions, metals identification and concentrations, as shown in Table 8. The adsorption experiments were conducted using 10 mg of fibers in 10 mL of wastewater for 2 h of contact time at room

temperature. A slight decrease is observed for some properties like pH and ions present in the real sample. The removal yield of the dye was up to 80%, with an adsorption capacity of 91 mg g^{-1}, showing that the adsorbent is effective in reducing the color of the wastewater.

4. Conclusions

A simple, green, and easy electrospinning method of PVA and L-cysteine blend has been performed to prepare promising membranes for dye removal. The morphology, structure and physico-chemical characterization show mat membranes with fiber diameters of ca. 179 nm (PVA) and 217 nm (PVA-CYS). The successful homogeneous incorporation of L-cysteine in PVA fibers is confirmed by FTIR spectroscopy and AFM phase imaging. Doehlert experimental design was adopted to evidence the effect of pH, amount of adsorbent and dye concentration on the adsorption process of CV on PVA and PVA-CYS. The two experimental designs show good correlations between experimental and predicted responses. It was found that the most influencing parameter is the pH for CV removal with PVA fibers. However, this parameter affects less the dye removal using PVA-CYS as adsorbent. This outcome is important for the large-scale application of this membrane since there is no need of effluent pH adjustment prior to treatment. The adsorption capacity of CV on PVA-CYS reached 197.21 mg g^{-1}, more than double of the adsorption capacity on PVA fibers, showing the good performance of the composite material. The effect of salinity and co-existing ions on the adsorption was negligible, demonstrating the membrane can work also in salted waters, whereas the spiking experiment demonstrated the membrane maintains a high efficiency in CV capture also in real wastewaters.

Fundings

The fundings of Ricerca Locale 2020 and Ricerca Locale 2021 are supplied by University of Turin.

Compliance with ethical standards

Not applicable.

Ethics approval

Not applicable.

Consent to participate

All authors participate to this work.

Consent for publication

All authors accept to publish this work.

CRediT authorship contribution statement

Eya Ben Khalifa: Conceptualization, Investigation, Methodology, Validation, Writing – original draft, Writing – review & editing. **Claudio Cecone:** Methodology, Investigation, Validation, Writing – review & editing. **Boutheina Rzig:** Investigation, Writing – review & editing. **Soulaima Azaiez:** Writing – review & editing. **Federico Cesano:** Investigation, Writing – review & editing. **Mery Malandrino:** Project administration, Writing – review & editing. **Pierangiola Bracco:** Supervision, Project administration, Writing – review & editing. **Giuliana Magnacca:** Supervision, Project administration, Funding acquisition, Writing – review & editing.

Declaration of Competing Interest

The authors have no competing interests to declare that are relevant to the content of this article.

Data availability

All data generated or analyzed during this study are included in this article.

Acknowledgements

- The authors acknowledge support from Project CH4.0 under MUR (Italian Ministry for the University) program “Dipartimenti di Eccellenza 2023-2027” (CUP: D13C22003520001)
- Special thanks to Professor Paola Calza for providing the real wastewater.

Appendix A. Supplementary data

Supplementary data to this article can be found online at https://doi.org/10.1016/j.reactfunctpolym.2023.105763.

References

[1] Dyes & Pigments Market Size & Share Report, 2030. https://www.grandviewresearch.com/industry-analysis/dyes-and-pigments-market, 2023 (accessed March 2, 2023).
[2] N. Sajn, Environmental Impact of the Textile and Clothing Industry: What Consumers Need to Know. https://policycommons.net/artifacts/1335345/environmental-impact-of-the-textile-and-clothing-industry/1941806/, 2019.
[3] M. Ağtaş, Ö. Yılmaz, M. Dilaver, K. Alp, İ. Koyuncu, Hot water recovery and reuse in textile sector with pilot scale ceramic ultrafiltration/nanofiltration membrane system, J. Clean. Prod. 256 (2020), 120359, https://doi.org/10.1016/j.jclepro.2020.120359.
[4] V. Jegatheesan, B.K. Pramanik, J. Chen, D. Navaratna, C.-Y. Chang, L. Shu, Treatment of textile wastewater with membrane bioreactor: a critical review, Bioresour. Technol. 204 (2016) 202–212, https://doi.org/10.1016/j.biortech.2016.01.006.
[5] D. Gautam, S. Hooda, Magnetic graphene oxide/chitin nanocomposites for efficient adsorption of methylene blue and crystal violet from aqueous solutions, J. Chem. Eng. Data 65 (2020) 4052–4062, https://doi.org/10.1021/acs.jced.0c00350.
[6] P. Kumari, M.K. Disha, D. Nayak, M.K. Dhruwe, S. Mishra Patel, Synthesis and characterization of sulfonated magnetic graphene-based cation exchangers for the removal of methylene blue from aqueous solutions, Ind. Eng. Chem. Res. 62 (2023) 1245–1256, https://doi.org/10.1021/acs.iecr.2c04432.
[7] J.M. Jabar, M.A. Adebayo, I.A. Owokotomo, Y.A. Odusote, M. Yılmaz, Synthesis of high surface area mesoporous ZnCl2–activated cocoa (Theobroma cacao L) leaves biochar derived via pyrolysis for crystal violet dye removal, Heliyon. 8 (2022), e10873, https://doi.org/10.1016/j.heliyon.2022.e10873.
[8] K. Mohanty, M. Jha, B.C. Meikap, M.N. Biswas, Removal of chromium (VI) from dilute aqueous solutions by activated carbon developed from Terminalia arjuna nuts activated with zinc chloride, Chem. Eng. Sci. 60 (2005) 3049–3059, https://doi.org/10.1016/j.ces.2004.12.049.
[9] S. Mani, R.N. Bharagava, Exposure to crystal violet, its toxic, genotoxic and carcinogenic effects on environment and its degradation and detoxification for environmental safety, in: W.P. de Voogt (Ed.), Reviews of Environmental Contamination and Toxicology 237, Springer International Publishing, Cham, 2016, pp. 71–104, https://doi.org/10.1007/978-3-319-23573-8_4.
[10] S. Mona, A. Kaushik, C.P. Kaushik, Waste biomass of Nostoc linckia as adsorbent of crystal violet dye: optimization based on statistical model, Int. Biodeterior. Biodegradation 65 (2011) 513–521, https://doi.org/10.1016/j.ibiod.2011.02.002.
[11] G.K. Cheruiyot, W.C. Wanyonyi, J.J. Kiplimo, E.N. Maina, Adsorption of toxic crystal violet dye using coffee husks: equilibrium, kinetics and thermodynamics study, Sci. Afr. 5 (2019), e00116, https://doi.org/10.1016/j.sciaf.2019.e00116.
[12] A. Mirza, R. Ahmad, An efficient sequestration of toxic crystal violet dye from aqueous solution by alginate/pectin nanocomposite: a novel and ecofriendly adsorbent, Groundw. Sustain. Dev. 11 (2020), 100373, https://doi.org/10.1016/j.gsd.2020.100373.
[13] G. Bal, A. Thakur, Distinct approaches of removal of dyes from wastewater: a review, Mater. Today: Proc. 50 (2022) 1575–1579, https://doi.org/10.1016/j.matpr.2021.09.119.
[14] Z. Yang, X. Liu, B. Gao, S. Zhao, Y. Wang, Q. Yue, Q. Li, Flocculation kinetics and floc characteristics of dye wastewater by polyferric chloride–poly-

epichlorohydrin–dimethylamine composite flocculant, Sep. Purif. Technol. 118 (2013) 583–590, https://doi.org/10.1016/j.seppur.2013.08.004.
[15] Y. Al-Ani, Y. Li, Degradation of C.I, Reactive blue 19 using combined iron scrap process and coagulation/flocculation by a novel Al(OH)3–polyacrylamide hybrid polymer, J. Taiwan Inst. Chem. Eng. 43 (2012) 942–947, https://doi.org/10.1016/j.jtice.2012.07.005.
[16] J. Dasgupta, J. Sikder, S. Chakraborty, S. Curcio, E. Drioli, Remediation of textile effluents by membrane based treatment techniques: a state of the art review, J. Environ. Manag. 147 (2015) 55–72, https://doi.org/10.1016/j.jenvman.2014.08.008.
[17] A.M.A. Abdelsamad, T.A. Gad-Allah, F.A. Mahmoud, M.I. Badawy, Enhanced photocatalytic degradation of textile wastewater using ag/ZnO thin films, journal of water, Process. Eng. 25 (2018) 88–95, https://doi.org/10.1016/j.jwpe.2018.07.002.
[18] I. Ibrahim, G.V. Belessiotis, A.M. Elseman, M.M. Mohamed, Y. Ren, T.M. Salama, M.B.I. Mohamed, Magnetic TiO2/CoFe2O4 Photocatalysts for degradation of organic dyes and pharmaceuticals without oxidants, Nanomaterials. 12 (2022) 3290, https://doi.org/10.3390/nano12193290.
[19] A. Ganeshkumar, D. Sivaraj, K. Vijayalakshmi, A. Vinothkannan, P. Raju, S. Dineshkumar, P. Santhanam, V. Ramalingam, R. Rajaram, Sunlight-irradiated bismuth titanate nanoparticles mediated degradation of methylene blue—ecological perspectives, Environ. Technol. Innov. 27 (2022), 102749, https://doi.org/10.1016/j.eti.2022.102749.
[20] W.S. Koe, J.W. Lee, W.C. Chong, Y.L. Pang, L.C. Sim, An overview of photocatalytic degradation: photocatalysts, mechanisms, and development of photocatalytic membrane, Environ. Sci. Pollut. Res. Int. 27 (2020) 2522–2565, https://doi.org/10.1007/s11356-019-07193-5.
[21] B. Sarkodie, J. Amesimeku, C. Frimpong, E.K. Howard, Q. Feng, Z. Xu, Photocatalytic degradation of dyes by novel electrospun nanofibers: a review, Chemosphere. 313 (2023), 137654, https://doi.org/10.1016/j.chemosphere.2022.137654.
[22] A.H. Alneyadi, M.A. Rauf, S.S. Ashraf, Oxidoreductases for the remediation of organic pollutants in water – a critical review, Crit. Rev. Biotechnol. 38 (2018) 971–988, https://doi.org/10.1080/07388551.2017.1423275.
[23] J. Zdarta, K. Jankowska, K. Bachosz, E. Kijeńska-Gawrońska, A. Zgoła-Grześkowiak, E. Kaczorek, T. Jesionowski, A promising laccase immobilization using electrospun materials for biocatalytic degradation of tetracycline: effect of process conditions and catalytic pathways, Catal. Today 348 (2020) 127–136, https://doi.org/10.1016/j.cattod.2019.08.042.
[24] Md.M. Hasan, M.A. Shenashen, Md.N. Hasan, H. Znad, Md.S. Salman, Md. R. Awual, Natural biodegradable polymeric bioadsorbents for efficient cationic dye encapsulation from wastewater, J. Mol. Liq. 323 (2021), 114587, https://doi.org/10.1016/j.molliq.2020.114587.
[25] R. Foroutan, S.J. Peighambardoust, S.H. Peighambardoust, M. Pateiro, J. M. Lorenzo, Adsorption of crystal violet dye using activated carbon of lemon wood and activated carbon/Fe3O4 magnetic nanocomposite from aqueous solutions: a kinetic, equilibrium and thermodynamic study, Molecules. 26 (2021) 2241, https://doi.org/10.3390/molecules26082241.
[26] A.S. Kamdod, M.V.P. Kumar, Adsorption of methylene blue, methyl orange, and crystal violet on microporous coconut shell activated carbon and its composite with chitosan: isotherms and kinetics, J. Polym. Environ. 30 (2022) 5274–5289, https://doi.org/10.1007/s10924-022-02597-w.
[27] Y. Tian, H. Ma, B. Xing, Preparation of surfactant modified magnetic expanded graphite composites and its adsorption properties for ionic dyes, Appl. Surf. Sci. 537 (2021), 147995, https://doi.org/10.1016/j.apsusc.2020.147995.
[28] Y.-H. Wu, K. Xue, Q.-L. Ma, T. Ma, Y.-L. Ma, Y.-G. Sun, W.-X. Ji, Removal of hazardous crystal violet dye by low-cost P-type zeolite/carbon composite obtained from in situ conversion of coal gasification fine slag, Microporous Mesoporous Mater. 312 (2021), 110742, https://doi.org/10.1016/j.micromeso.2020.110742.
[29] S.K. Shukla, S. Pandey, S. Saha, H.R. Singh, P.K. Mishra, S. Kumar, S.K. Jha, Removal of crystal violet by Cu-chitosan nano-biocomposite particles using Box–Behnken design, J. Environ. Chem. Eng. 9 (2021), 105847, https://doi.org/10.1016/j.jece.2021.105847.
[30] A. Djelad, A. Mokhtar, A. Khelifa, A. Bengueddach, M. Sassi, Alginate-whey an effective and green adsorbent for crystal violet removal: kinetic, thermodynamic and mechanism studies, Int. J. Biol. Macromol. 139 (2019) 944–954, https://doi.org/10.1016/j.ijbiomac.2019.08.068.
[31] X. Zhao, X. Wang, T. Lou, Simultaneous adsorption for cationic and anionic dyes using chitosan/electrospun sodium alginate nanofiber composite sponges, Carbohydr. Polym. 276 (2022), 118728, https://doi.org/10.1016/j.carbpol.2021.118728.
[32] S. Omer, L. Forgách, R. Zelkó, I. Sebe, Scale-up of electrospinning: market overview of products and devices for pharmaceutical and biomedical purposes, Pharmaceutics. 13 (2021) 286, https://doi.org/10.3390/pharmaceutics13020286.
[33] S.A. Hosseini, M.R. Samani, D. Toghraie, Investigating the hexavalent chromium removal from aqueous solution applying bee carcasses and corpses modified with polyaniline, Sci. Rep. 11 (2021) 19117, https://doi.org/10.1038/s41598-021-97518-7.
[34] Y. Kim, J. Park, J. Bang, J. Kim, J.-H. Kim, S.-W. Hwang, H. Yeo, I.-G. Choi, H. W. Kwak, Highly persistent lignocellulosic fibers for effective cationic dye pollutant removal, ACS Appl. Polym. Mater. 4 (2022) 6006–6020, https://doi.org/10.1021/acsapm.2c00837.
[35] X. Wang, J. Dong, C. Gong, S. Zhang, J. Yang, A. Zhang, Z. Feng, Bendable poly (vinylidene fluoride)/polydopamine/β-cyclodextrin composite electrospun membranes for highly efficient and bidirectional adsorption of cation and anion dyes from aqueous media, Compos. Sci. Technol. 219 (2022), 109256, https://doi.org/10.1016/j.compscitech.2021.109256.
[36] I. Santos-Sauceda, M.M. Castillo-Ortega, T. del Castillo-Castro, L. Armenta-Villegas, R. Ramírez-Bon, Electrospun cellulose acetate fibers for the photodecolorization of methylene blue solutions under natural sunlight, Polym. Bull. 78 (2021) 4419–4438, https://doi.org/10.1007/s00289-020-03324-y.
[37] H.-W. Leung, Ecotoxicology of glutaraldehyde: review of environmental fate and effects studies, Ecotoxicol. Environ. Saf. 49 (2001) 26–39, https://doi.org/10.1006/eesa.2000.2031.
[38] B. Dhandayuthapani, R. Mallampati, D. Sriramulu, R.F. Dsouza, S. Valiyaveettil, PVA/gluten hybrid nanofibers for removal of nanoparticles from water, ACS Sustain. Chem. Eng. 2 (2014) 1014–1021, https://doi.org/10.1021/sc500003k.
[39] C. Cecone, G. Hoti, M. Zanetti, F. Trotta, P. Bracco, Sustainable production of curable maltodextrin-based electrospun microfibers, RSC Adv. 12 (2022) 762–771, https://doi.org/10.1039/D1RA06785K.
[40] R. Salihu, S.I. Abd Razak, N. Ahmad Zawawi, M. Rafiq Abdul Kadir, N. Izzah Ismail, N. Jusoh, M. Riduan Mohamad, N. Hasraf Mat Nayan, Citric acid: a green cross-linker of biomaterials for biomedical applications, Eur. Polym. J. 146 (2021), 110271, https://doi.org/10.1016/j.eurpolymj.2021.110271.
[41] D. Nataraj, R. Reddy, N. Reddy, Crosslinking electrospun poly (vinyl) alcohol fibers with citric acid to impart aqueous stability for medical applications, Eur. Polym. J. 124 (2020), 109484, https://doi.org/10.1016/j.eurpolymj.2020.109484.
[42] P.G. Abadi, M. Irani, L.R. Rad, Mechanisms of the removal of the metal ions, dyes, and drugs from wastewaters by the electrospun nanofiber membranes, J. Taiwan Inst. Chem. Eng. 143 (2023), 104625, https://doi.org/10.1016/j.jtice.2022.104625.
[43] M. Xiao, J. Chery, M.W. Frey, Functionalization of electrospun poly(vinyl alcohol) (PVA) nanofiber membranes for selective chemical capture, ACS Appl. Nano Mater. 1 (2018) 722–729, https://doi.org/10.1021/acsanm.7b00180.
[44] S. Zhang, Q. Shi, G. Korfiatis, C. Christodoulatos, H. Wang, X. Meng, Chromate removal by electrospun PVA/PEI nanofibers: adsorption, reduction, and effects of co-existing ions, Chem. Eng. J. 387 (2020), 124179, https://doi.org/10.1016/j.cej.2020.124179.
[45] N. Mahanta, S. Valiyaveettil, Surface modified electrospun poly(vinyl alcohol) membranes for extracting nanoparticles from water, Nanoscale. 3 (2011) 4625–4631, https://doi.org/10.1039/C1NR10739A.
[46] C.W. Ooi, U. Waldo, Y. Norazriena, K.S. Lim, S.T. Tan, Z. Rozalina, H. Ahmad, L-cysteine grafted fiber-optic chemosensor for heavy metal detection, Opt. Fiber Technol. 71 (2022), 102938, https://doi.org/10.1016/j.yofte.2022.102938.
[47] D.F. Enache, E. Vasile, C.M. Simonescu, A. Răzvan, A. Nicolescu, A.-C. Nechifor, O. Oprea, R.-E. Pătescu, C. Onose, F. Dumitru, Cysteine-functionalized silica-coated magnetite nanoparticles as potential nanoadsorbents, J. Solid State Chem. 253 (2017) 318–328, https://doi.org/10.1016/j.jssc.2017.06.013.
[48] J. Mittal, R. Ahmad, M.O. Ejaz, A. Mariyam, A. Mittal, A novel, eco-friendly bio-nanocomposite (Alg-Cst/Kal) for the adsorptive removal of crystal violet dye from its aqueous solutions, Int. J. Phytoremed. 24 (2022) 796–807, https://doi.org/10.1080/15226514.2021.1977778.
[49] R.G. Moran-Salazar, G.G. Carbajal-Arizaga, J.A. Gutierréz-Ortega, J. Badillo-Camacho, R. Manríquez-González, I.G. Shenderovich, S. Gómez-Salazar, As(V) removal from aqueous media using an environmentally friendly zwitterion L-cysteine functionalized silica adsorbent, Chem. Eng. Sci. 278 (2023), 118879, https://doi.org/10.1016/j.ces.2023.118879.
[50] J. Jacyna, M. Kordalewska, M.J. Markuszewski, Design of Experiments in metabolomics-related studies: an overview, J. Pharm. Biomed. Anal. 164 (2019) 598–606, https://doi.org/10.1016/j.jpba.2018.11.027.
[51] G.E. De Benedetto, S. Di Masi, A. Pennetta, C. Malitesta, Response surface methodology for the optimisation of electrochemical biosensors for heavy metals detection, Biosensors. 9 (2019) 26, https://doi.org/10.3390/bios9010026.
[52] E. Ben Khalifa, B. Rzig, R. Chakroun, H. Nouagui, B. Hamrouni, Application of response surface methodology for chromium removal by adsorption on low-cost biosorbent, Chemom. Intell. Lab. Syst. 189 (2019) 18–26, https://doi.org/10.1016/j.chemolab.2019.03.014.
[53] P.S. Madamba, The response surface methodology: an application to optimize dehydration operations of selected agricultural crops, LWT Food Sci. Technol. 35 (2002) 584–592, https://doi.org/10.1006/fstl.2002.0914.
[54] B. Chalermsinsuwan, Y.-H. Li, K. Manatura, Optimization of gasification process parameters for COVID-19 medical masks using response surface methodology, Alex. Eng. J. 62 (2023) 335–347, https://doi.org/10.1016/j.aej.2022.07.037.
[55] S.M. Dadou, M.I. El-Barghouthi, M.D. Antonijevic, B.Z. Chowdhry, A.A. Badwan, Elucidation of the controlled-release behavior of metoprolol succinate from directly compressed xanthan gum/chitosan polymers: computational and experimental studies, ACS Biomater. Sci. Eng. 6 (2020) 21–37, https://doi.org/10.1021/acsbiomaterials.8b01028.
[56] L. El Faroudi, Y. El Jemli, R. Zari, A. Barakat, M.K. Ismael, K. Abdelouahdi, A. Solhy, Optimization of photocatalytic parameters using Doehlert experimental design to improve the photodegradation of Orange G, J. Photochem. Photobiol. A Chem. 445 (2023), 115012, https://doi.org/10.1016/j.jphotochem.2023.115012.
[57] S.T. Narenderan, S.N. Meyyanathan, V.V.S.R. Karri, Experimental design in pesticide extraction methods: a review, Food Chem. 289 (2019) 384–395, https://doi.org/10.1016/j.foodchem.2019.03.045.
[58] P.C.C. Faria, J.J.M. Orfão, M.F.R. Pereira, Adsorption of anionic and cationic dyes on activated carbons with different surface chemistries, Water Res. 38 (2004) 2043–2052, https://doi.org/10.1016/j.watres.2004.01.034.

[59] C. Cecone, G. Hoti, F. Caldera, M. Zanetti, F. Trotta, P. Bracco, NADES-derived beta cyclodextrin-based polymers as sustainable precursors to produce sub-micrometric cross-linked mats and fibrous carbons, Polym. Degrad. Stab. 202 (2022), 110040, https://doi.org/10.1016/j.polymdegradstab. 2022.110040.
[60] M.F. Barrera Vázquez, A.E. Andreatta, R.E. Martini, S.C. Núñez Montoya, J. L. Cabrera, L.R. Comini, Optimization of pretreatment with microwaves prior the pressurized hot water extraction of anthraquinones from Heterophyllaea pustulata, using Doehlert experimental design, Chem. Eng. Process. Process Intensif. 155 (2020), 108055, https://doi.org/10.1016/j.cep.2020.108055.
[61] U.M.F.M. Cerqueira, M.A. Bezerra, S.L.C. Ferreira, R. de Jesus Araújo, B.N. da Silva, C.G. Novaes, Doehlert design in the optimization of procedures aiming food analysis – a review, Food Chem. 364 (2021), 130429, https://doi.org/10.1016/j.foodchem.2021.130429.
[62] D. Feng, B. Bai, H. Wang, Y. Suo, Novel fabrication of PAA/PVA/yeast superabsorbent with interpenetrating polymer network for pH-dependent selective adsorption of dyes, J. Polym. Environ. 26 (2018) 567–588, https://doi.org/10.1007/s10924-017-0972-y.
[63] M. Thomas, S. Jose, Electrospun membrane of PVA and functionalized agarose with polymeric ionic liquid and conductive carbon for efficient dye sensitized solar cell, J. Photochem. Photobiol. A Chem. 425 (2022), 113666, https://doi.org/10.1016/j.jphotochem.2021.113666.
[64] A.S. Chatterley, P. Laity, C. Holland, T. Weidner, S. Woutersen, G. Giubertoni, Broadband multidimensional spectroscopy identifies the amide II vibrations in silkworm films, Molecules. 27 (2022) 6275, https://doi.org/10.3390/molecules27196275.
[65] S. Zhang, Q. Shi, C. Christodoulatos, X. Meng, Lead and cadmium adsorption by electrospun PVA/PAA nanofibers: batch, spectroscopic, and modeling study, Chemosphere. 233 (2019) 405–413, https://doi.org/10.1016/j.chemosphere.2019.05.190.
[66] W. Li, X. Li, Y. Chen, X. Li, H. Deng, T. Wang, R. Huang, G. Fan, Poly(vinyl alcohol)/sodium alginate/layered silicate based nanofibrous mats for bacterial inhibition, Carbohydr. Polym. 92 (2013) 2232–2238, https://doi.org/10.1016/j.carbpol.2012.12.004.
[67] Y. Hussein, E.M. El-Fakharany, E.A. Kamoun, S.A. Loutfy, R. Amin, T.H. Taha, S. A. Salim, M. Amer, Electrospun PVA/hyaluronic acid/L-arginine nanofibers for wound healing applications: nanofibers optimization and in vitro bioevaluation, Int. J. Biol. Macromol. 164 (2020) 667–676, https://doi.org/10.1016/j.ijbiomac.2020.07.126.
[70] V.H.B. Oliveira, F. Rechotnek, E.P. da Silva, V. de S Marques, A.F. Rubira, R. Silva, S.A. Lourenço, E.C. Muniz, A sensitive electrochemical sensor for Pb2+ ions based on ZnO nanofibers functionalized by L-cysteine, J. Mol. Liq. 309 (2020), 113041, https://doi.org/10.1016/j.molliq.2020.113041.
[71] M. Tripathy, S. Padhiari, G. Hota, L-cysteine-functionalized mesoporous magnetite Nanospheres: synthesis and adsorptive application toward arsenic remediation, J. Chem. Eng. Data 65 (2020) 3906–3919, https://doi.org/10.1021/acs.jced.0c00250.
[72] G. Göksen, M.J. Fabra, A. Pérez-Cataluña, H.I. Ekiz, G. Sanchez, A. López-Rubio, Biodegradable active food packaging structures based on hybrid cross-linked electrospun polyvinyl alcohol fibers containing essential oils and their application in the preservation of chicken breast fillets, Food Packag. Shelf Life 27 (2021), 100613, https://doi.org/10.1016/j.fpsl.2020.100613.
[73] N. Nikfarjam, N. Taheri Qazvini, Y. Deng, Cross-linked starch nanoparticles stabilized Pickering emulsion polymerization of styrene in w/o/w system, Colloid Polym. Sci. 292 (2014) 599–612, https://doi.org/10.1007/s00396-013-3102-y.
[74] V.S. Ghorpade, R.J. Dias, K.K. Mali, S.I. Mulla, Citric acid crosslinked carboxymethylcellulose-polyvinyl alcohol hydrogel films for extended release of water soluble basic drugs, J. Drug Del. Sci. Technol. 52 (2019) 421–430, https://doi.org/10.1016/j.jddst.2019.05.013.
[75] Z. Wu, C. Zhao, W. Zeng, X. Wang, C. Liu, Z. Yu, J. Zhang, Z. Qiu, Ultra-high selective removal of CR and Cr(VI) from aqueous solutions using polyethyleneimine functionalized magnetic hydrochar: application strategy and mechanisms insight, Chem. Eng. J. 448 (2022), 137464, https://doi.org/10.1016/j.cej.2022.137464.
[76] J. Uranga, I. Leceta, A. Etxabide, P. Guerrero, K. de la Caba, Cross-linking of fish gelatins to develop sustainable films with enhanced properties, Eur. Polym. J. 78 (2016) 82–90, https://doi.org/10.1016/j.eurpolymj.2016.03.017.
[77] A.D. Rajora, T. Bal, Evaluation of cashew gum-polyvinyl alcohol (CG-PVA) electrospun nanofiber mat for scarless wound healing in a murine model, Int. J. Biol. Macromol. 240 (2023), 124417, https://doi.org/10.1016/j.ijbiomac.2023.124417.
[78] S. Wu, K. Li, W. Shi, J. Cai, Preparation and performance evaluation of chitosan/polyvinylpyrrolidone/polyvinyl alcohol electrospun nanofiber membrane for heavy metal ions and organic pollutants removal, Int. J. Biol. Macromol. 210 (2022) 76–84, https://doi.org/10.1016/j.ijbiomac.2022.05.017.
[79] H. Fong, I. Chun, D.H. Reneker, Beaded nanofibers formed during electrospinning, Polymer. 40 (1999) 4585–4592, https://doi.org/10.1016/S0032-3861(99)00068-3.
[80] M. Marrese, V. Guarino, L. Ambrosio, Atomic force microscopy: a powerful tool to address scaffold design in tissue engineering, J. Funct. Biomater. 8 (2017) 7, https://doi.org/10.3390/jfb8010007.
[81] Phase Mode SPM/AFM, in: H. Nakajima, The Surface Science Society of Japan (Eds.), Compendium of Surface and Interface Analysis, Springer, Singapore, 2018, pp. 441–444, https://doi.org/10.1007/978-981-10-6156-1_72.
[82] D. Scarano, S. Bertarione, F. Cesano, G. Spoto, A. Zecchina, Imaging polycrystalline and smoke MgO surfaces with atomic force microscopy: a case study of high resolution image on a polycrystalline oxide, Surf. Sci. 570 (2004) 155–166, https://doi.org/10.1016/j.susc.2004.07.024.
[83] M.I. Hassan, N. Sultana, Characterization, drug loading and antibacterial activity of nanohydroxyapatite/polycaprolactone (nHA/PCL) electrospun membrane, 3, Biotech. 7 (2017) 249, https://doi.org/10.1007/s13205-017-0889-0.
[84] M. Harahap, Y.A. Perangin-Angin, V. Purwandari, R. Goei, A. Ling Y. Tok, S. Gea, Acetylated lignin from oil palm empty fruit bunches and its electrospun nanofibres with PVA: potential carbon fibre precursor, Heliyon. 9 (2023), e14556, https://doi.org/10.1016/j.heliyon.2023.e14556.
[85] N. Azeez Betti, Thermogravimetric analysis on PVA / PVP blend under air atmosphere, ETJ. 34 (2016) 2433–2442, https://doi.org/10.30684/etj.34.13A.6.
[86] B.J. Holland, J.N. Hay, The thermal degradation of poly(vinyl alcohol), Polymer. 42 (2001) 6775–6783, https://doi.org/10.1016/S0032-3861(01)00166-5.
[87] N.A.H. Rosli, K.S. Loh, W.Y. Wong, T.K. Lee, A. Ahmad, Hybrid composite membrane of phosphorylated chitosan/poly (vinyl alcohol)/silica as a proton exchange membrane, Membranes. 11 (2021) 675, https://doi.org/10.3390/membranes11090675.
[88] J. Antony, 4 - a systematic methodology for Design of Experiments, in: J. Antony (Ed.), Design of Experiments for Engineers and Scientists, Second edition, Elsevier, Oxford, 2014, pp. 33–50, https://doi.org/10.1016/B978-0-08-099417-8.00004-3.
[89] H. Douahem, H. Hammi, A. Hamzaoui, M. Adel, Modeling and optimization of phosphogypsum transformation into calcium fluoride using experimental design methodology, J. Tunisian Chem. Soc. 18 (2016) 106–113.
[90] M.K. Uddin, N.N. Abd Malek, A.H. Jawad, S. Sabar, Pyrolysis of rubber seed pericarp biomass treated with sulfuric acid for the adsorption of crystal violet and methylene green dyes: an optimized process, Int. J. Phytoremed. 25 (2023) 393–402, https://doi.org/10.1080/15226514.2022.2086214.
[91] H. Kandil, H. Ali, Simultaneous removal of cationic crystal violet and anionic reactive yellow dyes using eco-friendly chitosan functionalized by talc and Cloisite 30B, J. Polym. Environ. 31 (2023) 1456–1477, https://doi.org/10.1007/s10924-022-02682-0.
[92] V. Manzo, O. Navarro, L. Honda, K. Sánchez, M. Inés Toral, P. Richter, Determination of crystal violet in water by direct solid phase spectrophotometry after rotating disk sorptive extraction, Talanta. 106 (2013) 305–308, https://doi.org/10.1016/j.talanta.2012.11.004.
[93] K.M. Elsherif, Abdelmeneim El-Dali, A.A. Alkarewi, Abdunaser Mabrok Ewlad-Ahmed, A. Treban, Adsorption of Crystal Violet Dye onto Olive Leaves Powder: Equilibrium and Kinetic Studies, 2021, https://doi.org/10.5281/ZENODO.4441851.
[94] N. Salahuddin, M.A. Abdelwahab, A. Akelah, M. Elnagar, Adsorption of Congo red and crystal violet dyes onto cellulose extracted from Egyptian water hyacinth, Nat. Hazards 105 (2021) 1375–1394, https://doi.org/10.1007/s11069-020-04358-1.
[95] P.B. Krishnappa, A.K. Kodoth, P. Kulal, V. Badalamoole, Effective removal of ionic dyes from aqueous media using modified karaya gum–PVA semi-interpenetrating network system, Polym. Bull. 80 (2023) 2553–2584, https://doi.org/10.1007/s00289-022-04169-3.
[96] Y.S. Al-Degs, M.I. El-Barghouthi, A.H. El-Sheikh, G.M. Walker, Effect of solution pH, ionic strength, and temperature on adsorption behavior of reactive dyes on activated carbon, Dyes Pigments 77 (2008) 16–23, https://doi.org/10.1016/j.dyepig.2007.03.001.
[97] J. Xie, R. Lin, Z. Liang, Z. Zhao, C. Yang, F. Cui, Effect of cations on the enhanced adsorption of cationic dye in Fe3O4-loaded biochar and mechanism, J. Environ. Chem. Eng. 9 (2021), 105744, https://doi.org/10.1016/j.jece.2021.105744.
[98] H.N. Tran, Y.-F. Wang, S.-J. You, H.-P. Chao, Insights into the mechanism of cationic dye adsorption on activated charcoal: the importance of π–π interactions, Process. Saf. Environ. Prot. 107 (2017) 168–180, https://doi.org/10.1016/j.psep.2017.02.010.
[99] R. Ahmad, K. Ansari, Fabrication of alginate@silver nanoparticles (Alg@AgNPs) bionanocomposite for the sequestration of crystal violet dye from aqueous solution, Int. J. Biol. Macromol. 218 (2022) 157–167, https://doi.org/10.1016/j.ijbiomac.2022.07.092.
[100] M. Mozaffari Majd, V. Kordzadeh-Kermani, V. Ghalandari, A. Askari, M. Sillanpää, Adsorption isotherm models: a comprehensive and systematic review (2010−2020), Sci. Total Environ. 812 (2022), 151334, https://doi.org/10.1016/j.scitotenv.2021.151334.
[101] H.T. Nguyen, F.A. Ngwabebhoh, N. Saha, T. Saha, P. Saha, Gellan gum/bacterial cellulose hydrogel crosslinked with citric acid as an eco-friendly green adsorbent for safranin and crystal violet dye removal, Int. J. Biol. Macromol. 222 (2022) 77–89, https://doi.org/10.1016/j.ijbiomac.2022.09.040.
[102] H. Kandil, H. Ali, Simultaneous removal of cationic crystal violet and anionic reactive yellow dyes using eco-friendly chitosan functionalized by talc and Cloisite 30B, J. Polym. Environ. 31 (2023) 1456–1477, https://doi.org/10.1007/s10924-022-02682-0.
[103] K. Mohanty, J.T. Naidu, B.C. Meikap, M.N. Biswas, Removal of crystal violet from wastewater by activated carbons Prepared from Rice husk, Ind. Eng. Chem. Res. 45 (2006) 5165–5171, https://doi.org/10.1021/ie060257r.
[104] R. Ahmad, K. Ansari, Polyacrylamide-grafted Actinidia deliciosa peels powder (PGADP) for the sequestration of crystal violet dye: isotherms, kinetics and thermodynamic studies, Appl Water Sci 10 (2020) 195, https://doi.org/10.1007/s13201-020-01263-7.
[105] R. Ahmad, M.O. Ejaz, Efficient adsorption of crystal violet (CV) dye onto benign chitosan-modified l-cysteine/bentonite (CS-Cys/bent) bionanocomposite: synthesis, characterization and experimental studies, Dyes Pigments 216 (2023), 111305, https://doi.org/10.1016/j.dyepig.2023.111305.

[106] Y. Li, S. Wang, Z. Shen, X. Li, Q. Zhou, Y. Sun, T. Wang, Y. Liu, Q. Gao, Gradient adsorption of methylene blue and crystal violet onto compound microporous silica from aqueous medium, ACS Omega 5 (2020) 28382–28392, https://doi.org/10.1021/acsomega.0c04437.
[107] M.A. Al-Ghouti, R.S. Al-Absi, Mechanistic understanding of the adsorption and thermodynamic aspects of cationic methylene blue dye onto cellulosic olive stones biomass from wastewater, Sci. Rep. 10 (2020) 15928, https://doi.org/10.1038/s41598-020-72996-3.
[108] S. Bibi, A. Bibi, M.N. Mullungal, M. Abu-Dieyeh, M.A. Al-Ghouti, Macroalgae as an eco-friendly and successful green technology for the removal of crystal violet from synthetic and real wastewater, Arab. J. Chem. 16 (2023), 105191, https://doi.org/10.1016/j.arabjc.2023.105191.
[109] M.O. Ani, M.C. Menkiti, C.O. Aniagor, C.E. Nworie, D.O. Ochi, Canarium schweinfurthii stone-derived biochar: a promising adsorbent for crystal violet dye removal, Res. Surf. Interf. 12 (2023), 100144, https://doi.org/10.1016/j.rsurfi.2023.100144.
[110] A. Jebli, A.E. Amri, R. Hsissou, A. Lebkiri, B. Zarrik, F.Z. Bouhassane, E. Mahdi Hbaiz, E.H. Rifi, A. Lebkiri, Synthesis of a chitosan@hydroxyapatite composite hybrid using a new approach for high-performance removal of crystal violet dye in aqueous solution, equilibrium isotherms and process optimization, J. Taiwan Inst. Chem. Eng. 149 (2023), https://doi.org/10.1016/j.jtice.2023.105006, 105006.
[111] J. Cheriaa, M. Khaireddine, M. Rouabhia, A. Bakhrouf, Removal of triphenylmethane dyes by bacterial consortium, ScientificWorldJournal. 2012 (2012), 512454, https://doi.org/10.1100/2012/512454.
[112] K. Belkassa, M. Khelifa, I. Batonneau-Gener, K. Marouf-Khelifa, A. Khelifa, Understanding of the mechanism of crystal violet adsorption on modified halloysite: hydrophobicity, performance, and interaction, J. Hazard. Mater. 415 (2021), 125656, https://doi.org/10.1016/j.jhazmat.2021.125656.
[113] D. Yu, Y. Wang, M. Wu, L. Zhang, L. Wang, H. Ni, Surface functionalization of cellulose with hyperbranched polyamide for efficient adsorption of organic dyes and heavy metals, J. Clean. Prod. 232 (2019) 774–783, https://doi.org/10.1016/j.jclepro.2019.06.024.
[114] B.R. Iyer, R. Mahalakshmi, Hydrophobic characteristic is energetically preferred for cysteine in a model membrane protein, Biophys. J. 117 (2019) 25–35, https://doi.org/10.1016/j.bpj.2019.05.024.